Pyrolysis oil composition and catalytic activity estimated by cumulative mass analysis using Py-GC/MS EGA-MS

Ryan D. Merckel[a], Mike D. Heydenrych[a], Bruce B. Sithole[b,c]

[a]*Department of Chemical Engineering, University of Pretoria, Pretoria, South Africa*
[b]*Biorefinery Industry Development Facility, Council for Scientific & Industrial Research, Durban, South Africa*
[c]*Discipline of Chemical Engineering, University of KwaZulu-Natal, Durban, South Africa*

ABSTRACT

An advancement in the analytical capabilities of pyrolysis-gas chromatography/mass spectrometry (Py-GC/MS) with evolved gas analysis-mass spectrometry (EGA-MS) is presented. The combined method of analysis can predict elemental composition and calorific content of pyrolysis products using linear regression between the mass fractions of elemental entities and the mass fractions of their respective compounds. The method also reduces the need for elemental analysis, bomb calorimetry, and Karl Fischer titration. Elemental compositions obtained from literature with a low level of characterisation of 29 % could be estimated with a mean absolute error (MAE) of 6.1 %, while calorific values could be predicted within a MAE of 3.5 MJ kg^{-1}. The performance of various catalysts in upgrading *Eucalyptus grandis* sawdust-derived pyrolysis oil was also demonstrated with this method, whereby the mechanisms, changes to elemental composition, and impact on calorific value were assessed. It was found that catalytic fast pyrolysis by the calcium-aluminium layered double oxide (Ca-Al-LDO) is dominated by decarboxylation, with a dehydration to decarboxylation ratio of H_2O/CO_2 = 0.18, compared to the magnesium-aluminium layered double oxide (Mg-Al-LDO) (H_2O/CO_2 = 1.29) and bentonite (H_2O/CO_2 = 0.82). ZSM-5 on the other hand achieved decarboxylation by the dominant mechanism of dehydration, with H_2O/CO_2 = 3.55.

Keywords: Py-GC/MS, fast pyrolysis, catalysis, estimation

Nomenclature

Symbol	Description	Units
A	Massic species or massic dataset	
A^*	Final predicted mass location with respect to entity A	
B	Massic dataset of entity B	
B^*	Final predicted mass location with respect to entity B	
C	Massic dataset of entity C	
C^*	Final predicted mass location with respect to entity C	
D	Massic dataset of entity D	
D^*	Final predicted mass location with respect to entity D	
E	Massic dataset of entity E	
E^*	Final predicted mass location with respect to entity E	
i	Lower index of summation or an entity	
j	Upper index of summation or an entity	
m	Mass quantity	kg
m_A	Mass quantity of entity A	$\mathrm{kg_A}$
m_{A_i}	Mass quantity of entity A in molecule i	$\mathrm{kg_{A_i}}$
m_{C_i}	Mass quantity of carbon	$\mathrm{kg_{C_i}}$
m_{H_i}	Mass quantity of hydrogen	$\mathrm{kg_{H_i}}$
m_i	Mass quantity of molecule i	kg_i or %
M_{C}	Molar mass of elemental carbon	$\mathrm{kg_C\ kmol_C^{-1}}$
M_{H}	Molar mass of elemental hydrogen	$\mathrm{kg_H\ kmol_H^{-1}}$
M_i	Molar mass of entity i	$\mathrm{kg}_i\ \mathrm{kmol}_i^{-1}$
M_{O}	Molar mass of elemental oxygen	$\mathrm{kg_O\ kmol_O^{-1}}$
M_{O_2}	Molar mass of diatomic oxygen	$\mathrm{kg_{O_2}\ kmol_{O_2}^{-1}}$
m_{O_i}	Mass quantity of oxygen	$\mathrm{kg_{O_i}}$
R^2	Coefficient of determination	
X_i	True entity of i	
Y_i	Predicted entity i	
$\Delta_c h^\circ\vert_{\mathrm{HHV}}$	Standard massic combustion enthalpy	$\mathrm{MJ\ kg^{-1}}$
ν_{C}	Stoichiometric entity of carbon	
ν_{H}	Stoichiometric entity of hydrogen	
ν_{O}	Stoichiometric entity of oxygen	
ω_A	Mass fraction of entity A	$\mathrm{kg}_A\ \mathrm{kg_{total}^{-1}}$
ω_{C}	Mass fraction of carbon	$\mathrm{kg_C\ kg_{total}^{-1}}$
ω_{H}	Mass fraction of hydrogen	$\mathrm{kg_H\ kg_{total}^{-1}}$
ω_{O}	Mass fraction of oxygen	$\mathrm{kg_O\ kg_{total}^{-1}}$

1. Introduction

The pyrolytic decomposition of biomass via charring, depolymerization and fragmentation creates products of biochar, pyrolysis oil and synthesis gas that are in part reminiscent of the parent feedstock [1–3]. Similarities in elemental composition and calorific value are apparent when the biomass feedstock and its respective pyrolysis oil are compared, since pyrolysis oils tend to have calorific values similar to the feedstock that produced them. The higher heating value of pyrolysis oils derived from woody biomass feedstocks is typically lower (between 15 $\mathrm{MJ\,kg^{-1}}$ and 20 $\mathrm{MJ\,kg^{-1}}$) compared to conventional fuels (between 42 $\mathrm{MJ\,kg^{-1}}$ and 45 $\mathrm{MJ\,kg^{-1}}$) due to the presence of oxygenates[4]. Further upgradation of pyrolysis oil is required to increase its energy quality and physical properties relative to its parent feedstock[5], as it is inherently unstable and incompatible for use as a fuel in existing energy technologies and infrastructure. Filtration is used to reduce solid particulate matter, especially biochar, while homogenization may be achieved through blending pyrolysis oil with solvents and also decreases instability and viscosity[6,7]. Emulsification of pyrolysis oils with conventional fuels such as diesel with the addition of surfactants has also been reported[8,9]. While these methods aim to improve the physical properties of pyrolysis oils, the calorific potential and constituency of pyrolysis oils remained relatively unaltered.

Catalytic upgradation differs in that it aims to modify the constituents of pyrolysis oils through catalytic vapour cracking[10], hydrotreating[11], esterification[12], and gasification for the production of Fischer-Tropsch liquids[13]. Nolte & Shanks[14] are of the opinion that high oxygen contents in pyrolysis oils are the cause for the major challenges in utilizing pyrolysis oils. This is partially in contrast to the theory presented by Venderbosch[15] who suggests that oxygen is not necessarily a direct measure of pyrolysis oil quality since increases in viscosity are observed following dehydration. Regardless of opinion, catalyst development for upgrading pyrolysis oils remains the focal point and bottleneck for fast pyrolysis research. For instance, catalytic pyrolysis of woody biomass using zeolite-type catalysts is common, where zeolites selectively isomerize aromatics, aromatize low molecular weight oxygenates such as acids, alcohols, aldehydes, and deoxygenate aromatic compounds derived from the pyrolytic depolymerization of lignin[16–19]. The conversion of glucose, the monomer that constitutes cellulose, to platform chemicals has also been demonstrated via zeolite catalysis[20]. Zeolites have for some time now been the go-to catalyst for upgrading pyrolysis oils, and research in this area has focused strongly on their modification, such as the incorporation of transition metals, surface modifications by chemical deposition, or altering the acidity of the catalyst by varying the Si:Al ratio. But while the modification of zeolites has improved their performance, more is needed to overcome the limitations that are inherent to zeolites. The search for a single-step route for upgrading complex pyrolysis oils is yet another dilemma that may require not only bifunctional and/or multiple types of catalyst, but also better process design and catalyst handling[21,22]. What is needed is for catalyst design to be more focused on improved catalyst performance towards cracking, with deoxygenation via decarboxylation being targeted by limited hydrogen and carbon reduction, and by resistance against deactivation via coking, *etc*.[23].

Py-GC/MS is a useful and convenient tool for research in catalytic fast pyrolysis, as quantitative investigations of product distributions following catalytic fast pyrolysis are easily completed over a wide range of temperatures, residence times, and screening various types of catalysts with minimal effort is possible [24–28]. This technique achieves the quantification of pyrolysis volatiles using only small sample sizes in the milligram range and is especially valuable where materials with catalytic potential are expensive, and where materials & equipment available to perform pyrolysis experiments are limited or inaccessible. The ability to separate volatile pyrolysis products in the gas phase and identify them via GC/MS makes the analytical technique of Py-GC/MS a powerful method for the identification and quantification of chemical constituents, approximation of syringol-guaiacol ratios associated with lignin

pyrolysis, activity and selectivity of catalytic materials [26,28,29], and optimization of selectivity towards desired compounds[30]. However, the technique is not without its limitations. If additional information pertaining to the physical properties of pyrolysis oil is required such as elemental composition on a dry basis for the approximation of the higher heating value[31,32], additional analytical techniques need to be employed—this usually also requires larger sample sizes. For instance, both the determination of the heat of combustion and elemental composition on a dry basis requires moisture to be determined via volumetric Karl Fischer titration due to the high moisture content of pyrolysis oils. But the composition of pyrolysis oils can also negatively impact the accuracy Karl Fischer titration unless the resulting analytical disturbances are adequately supressed[33]. This may possibly introduce inaccuracies to the other analyses unknowingly. GC/MS analysis on the other hand may be able to generate these same data as characterisation of pyrolysis oil components is achieved with minimal moisture interference, but is limited by the availability of and access to standard reference spectra, successful comparison of these spectra with and identification of the generated spectra, and the sophistication of the software being used to accomplish this[34].

With the use of appropriate assumptions, this work proposes an indirect method of analysis that uses Py-GC/MS data to estimate the calorific value, extent of deoxygenation, elemental composition and extent of catalytic upgradation of pyrolysis oils without the added requirement of additional analytical techniques such as bomb calorimetry and elemental analysis. The proposed method is derived theoretically, demonstrated using modelled data, validated with data from the literature, and then applied to the catalytic upgrading of pyrolysis oils. An outline of this study is shown in Figure 1.

2. Derivation of model	3. Materials and method	4. Results and discussion	5. Conclusions
• Equations are derived based on conservation of mass. • Pseudo-GC/MS data generated and model is validated. • Sensitivity analysis of model completed.	• Materials: Choice of feedstock and catalysts presented. • Method: Py-GC/MS used with presented method of analysis.	• Method of analysis applied to four pyrolysis oils generated via Py-GC/MS. • Results are discussed.	

Figure 1: Outline of the format structure of this study.

2. Derivation of model

In the derivation of the proposed model, the following assumptions are made:

a. The products of pyrolysis are reminiscent of the parent feedstock.

b. Gaseous compounds that remain in the gas phase at ambient conditions are not considered as part of the liquid fraction.

c. Isomeric variations of molecules have a negligible effect on the overall calorific value and elemental composition of the pyrolysis oil.

d. For simplicity of the validation and application of the methods, all compounds' calorific values can be estimated using the correlation of Merckel *et al.*[32,35] – noting that the measured calorific values could also be found in the literature if available.

e. The products of pyrolysis are commutative and associative with respect to each other.

f. The conservation of mass holds, such that if all compounds present in a pyrolysis sample are fully characterised via GC/MS, it is possible to determine the individual masses of each element fully as well. These results should not contradict data obtained from elemental analysis.

The proposed method is introduced procedurally thus:

a. The mathematical derivation is derived using the above-mentioned assumptions and the procedure for its application is described.

b. GC chromatograms are generated using 357 data sourced from literature[36,37] for use as "pseudo-GC/MS" datasets. These pseudo-GC/MS datasets are produced using a randomized approach in the determination of the mass percentages of each compound, against which the efficacy of the method is demonstrated. Since all molecular formulae and calorific values of the compounds are therefore known and mass is conserved, it is also possible to test the sensitivity of the developed model in the case where only a fraction of compounds is being used to estimate properties.

c. The method is applied to 19 sets of data from the literature[38–44] that adequately describe the elemental compositions and calorific values of pyrolysis oils.

d. The method is used in the analysis of catalysts evaluated for their effectiveness in upgrading pyrolysis oil produced from *Eucalyptus grandis* wood.

2.1. Indirect methods for determination of mass distributions and HHV

The mass fraction of entity A is defined as

$$\frac{m_A}{m} = \omega_A \tag{1}$$

and the mass fraction of entity A in molecule i is similarly defined as

$$\frac{m_{A_i}}{m_i} = \omega_{A_i} \tag{2}$$

Equation 1 and Equation 2 are related by

$$\omega_A = \frac{m_A}{m} = \frac{m_{A_1} + m_{A_2} + \cdots + m_{A_{n-1}} + m_{A_n}}{m_1 + m_2 + \cdots + m_{n-1} + m_n} = \frac{\sum_{i=1}^{n} m_{A_i}}{\sum_{i=1}^{n} m_i} = \sum_{i=1}^{n} \frac{m_{A_i}}{m_i} = \sum_{i=1}^{n} \omega_{A_i}$$

Therefore, the mass of entity A, $m_A = \sum_{i=1}^{n} m_{A_i}$, can been determined as

$$\sum_{i=1}^{n} m_{A_i} = \frac{m_A}{m} \sum_{i=1}^{n} m_i \tag{3}$$

which is simply a mass balance with respect to component A in accordance with the law of mass conservation. Equation 3 describes the ideal case where all n entities are known, whereas in the case of limited characterisation of the pyrolytic product, only j entities are known. Equation 3 can be rewritten to reflect this as

$$\sum_{i=1}^{n} m_{A_i} = \frac{m_A}{m} \sum_{i=1}^{j} m_i + \frac{m_A}{m} \sum_{i=j+1}^{n} m_i$$

where $\frac{m_A}{m} \sum_{i=j+1}^{n} m_i$ denotes the sum of all unidentified entities within a set. Also,

$$\sum_{i=1}^{j} m_{A_i} = \frac{m_A}{m} \sum_{i=1}^{j} m_i \quad (4)$$

By applying the assumption that pyrolytic products are reminiscent of their parent feedstock, m_A may be approximated as

$$m_A = \sum_{i=1}^{n} m_{A_i} \approx \frac{m_A}{m} \sum_{i=1}^{j} m_i \quad (5)$$

and since

$$\frac{m_A}{m} = \omega_A$$

Equation 5 becomes

$$\sum_{i=1}^{n} m_{A_i} \approx \omega_A \sum_{i=1}^{j} m_i \quad (6)$$

The mass fraction of component A within a pyrolytic product, ω_A, may therefore be estimated using Equation 5 by plotting the sum of the known elemental mass fractions of component A $\left(\omega_A \sum_{i=1}^{j} m_i\right)$ against the sum of the respective mass fractions of component A, $\left(\sum_{i=1}^{n} m_{A_i}\right)$. On a basis of $m_A = 100$ massic units, the total mass of component A in the pyrolytic product can be determined by extrapolation by setting $\sum_{i=1}^{j} m_i = 100$, which corresponds with $j \to n$, to yield

$$m_A \approx \omega_A(100) \quad (7)$$

Since ω_A represents the gradient of Equation 6, a graphical linear regression may be used to find ω_A and thereby estimate m_A, in a similar manner to how bomb calorimetry measures and follows the rise in temperature after ignition to determine the calorific value of combustible materials[45].

2.2. Generation of pseudo-GC/MS data

Pseudo-GC/MS chromatograms are generated to test the indirect method of analysis for the determination of mass distributions and HHV. This is achieved through sorting the 357 data sourced from literature [33,34] into three sets comprising compounds of low, moderate and high oxygen content on the molar basis. The average higher heating values (HHV: $\Delta_c h^\circ\big|_{\mathrm{HHV}}$) for these data ($\Delta_c h^\circ\big|_{\mathrm{HHV}} \sim -27.5\ \mathrm{MJ\ kg^{-1}}$) is used to apportion each datum to a set. Compounds with a mole ratio for oxygen (ν_{O}) and carbon (ν_{C}) of $\nu_{\mathrm{O}}/\nu_{\mathrm{C}} \geq 0.67$ (corresponding to $\Delta_c h^\circ\big|_{\mathrm{HHV}} < 0.5 \times -27.5\ \mathrm{MJ\ kg^{-1}} = -13.8\ \mathrm{MJ\ kg^{-1}}$) are classified as highly-oxidised compounds. Those compounds with a mole ratio $0.21 < \nu_{\mathrm{O}}/\nu_{\mathrm{C}} < 0.67$ ($-13.8\ \mathrm{MJ\ kg^{-1}} < \Delta_c h^\circ\big|_{\mathrm{HHV}} < -27.5\ \mathrm{MJ\ kg^{-1}}$) are classified as moderately-oxidised compounds, while the remaining compounds with a mole ratio $\nu_{\mathrm{O}}/\nu_{\mathrm{C}} \leq 0.21$ ($\Delta_c h^\circ\big|_{\mathrm{HHV}} > 1.5 \times -27.5\ \mathrm{MJ\ kg^{-1}} = -41.3\ \mathrm{MJ\ kg^{-1}}$) are classified as either sparsely-oxidised or oxygen-free compounds.

Compounds are assigned randomised simulated peak intensity of arbitrary units (a.u.) which have been normalised against the maximum peak-intensity value within each data set. Additionally, each compound is assigned a randomised consecutive retention time in order to plot the chromatograms for each set (Figure 2). The resulting equivalent molecular formulae and higher heating values associated with each set are $\mathrm{C_{1.00}H_{1.73}O_{0.08}}$ and $\Delta_c h^\circ = -41.2\ \mathrm{MJ\ kg^{-1}}$ (low oxygen content), $\mathrm{C_{1.00}H_{1.64}O_{0.35}}$ and $\Delta_c h^\circ = -28.6\ \mathrm{MJ\ kg^{-1}}$ (moderate oxygen content), and $\mathrm{C_{1.00}H_{1.70}O_{0.91}}$ and $\Delta_c h^\circ = -15.3\ \mathrm{MJ\ kg^{-1}}$ (high oxygen content), respectively.

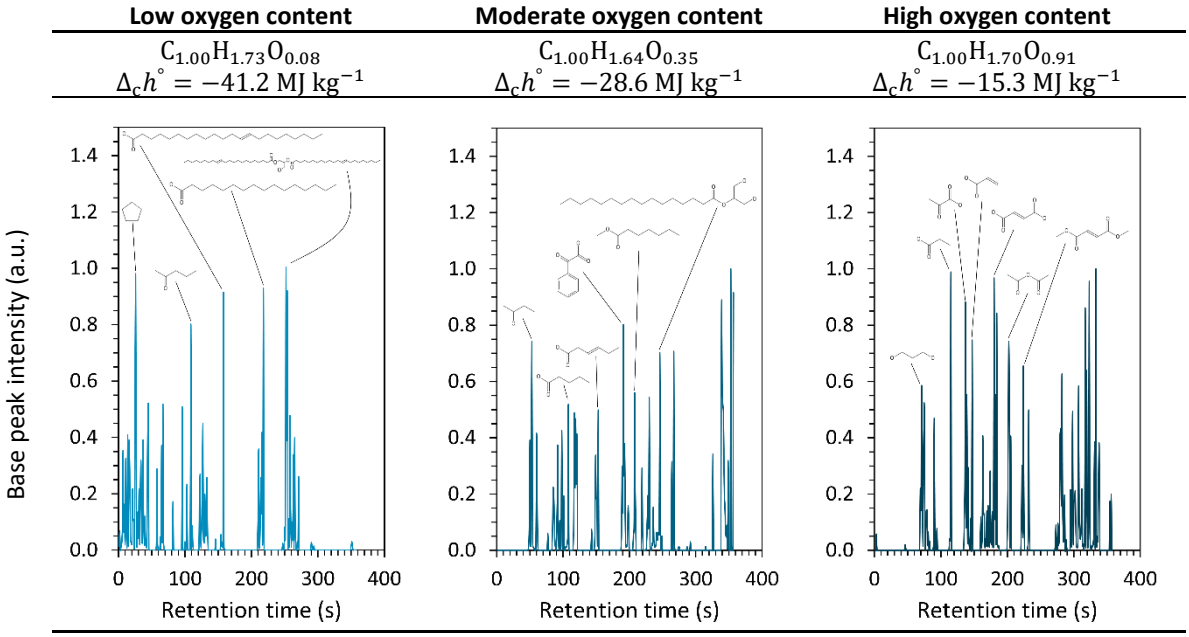

Figure 2: Plot of randomly generated pseudo-GC/MS chromatograms for compounds with oxygen content ranging from low (left), moderate (middle) and high (right).

2.3. Validation of models using pseudo GC/MS data

2.3.1. Validation of the proposed method

The data generated for the pseudo GC/MS chromatograms are sorted within each set from the smallest to the largest mass contribution before plotting the mass fractions per compound cumulatively for carbon, $\sum_{i=1}^{j} m_{\mathrm{C}_i}$, hydrogen, $\sum_{i=1}^{j} m_{\mathrm{H}_i}$, and oxygen, $\sum_{i=1}^{j} m_{\mathrm{O}_i}$, against the cumulative mass fraction for each datum, $\sum_{i=1}^{j} m_i$, according to Equation 6. Linear regression is used to determine the gradient for each trend in the data, which corresponds to the total mass fraction of the respective element (i.e. carbon, hydrogen, and oxygen) present in the entire pyrolytic product (Figure 3, left). Strong linear correlations between the cumulative elemental mass fractions and the cumulative mass fractions are observed for all data sets, and confirms the reasonability of the assumptions applied, namely that pyrolytic products are commutative and associative to each other, and that pyrolytic products are reminiscent of their parent feedstock. A sensitivity analysis was used to test the accuracy of Equation 6 when less than 100 % of molecular entities are known. Various subsets of the data were selected comprising 80 %, 60 %, 40 % and 20 % of the original data, and linear regression was used to determine deviations in predicting elemental mass fractions (Figure 3, right) and the higher heating values (Table 1). The higher heating values are calculated using the following equation [31,32]:

$$\Delta_c h^\circ = -13.87 \times M_{\mathrm{O}_2} \times \left(\frac{\omega_{\mathrm{C}}}{M_{\mathrm{C}}} + 0.25 \frac{\omega_{\mathrm{H}}}{M_{\mathrm{H}}} - 0.5 \frac{\omega_{\mathrm{O}}}{M_{\mathrm{O}}} \right) \quad \mathrm{MJ\ kg^{-1}} \tag{8}$$

where M_i refers to the molar mass of entity i. Deviations were measured using the mean absolute error (MAE) defined as

$$\mathrm{MAE} = \sum_{i=1}^{n} \frac{1}{n} |Y_i - X_i| \tag{9}$$

where Y_i is the prediction and X_i is the true value, with MAE taking on the same units as the values used.

Table 1: Sensitivity analyses for calorific values using indirect mass predication method II with limited datasets.

Degree of characterisation	Higher heating value $(\mathbf{MJ\ kg^{-1}})$			Mean absolute error $(\mathbf{MJ\ kg^{-1}})$		
	Low oxygen	Moderate oxygen	High oxygen	Low oxygen	Moderate oxygen	High oxygen
100 %, reference	−41.2	−28.6	−15.3	—	—	—
100 %	−41.1	−30.3	−15.2	0.1	1.6	0.1
80 %	−41.1	−29.0	−15.2	0.2	0.4	0.0
60 %	−41.2	−28.8	−15.3	0.0	0.2	0.1
40 %	−41.1	−29.0	−15.5	0.1	0.4	0.2
20 %	−39.5	−28.3	−15.0	1.7	0.4	0.3

2.3.2.Validation using data from literature

It is expected that elemental compositions and calorific values reported in the literature will provide a more stringent basis for evaluating the indirect method of prediction presented in this work. For this purpose, literature sources that meet the following criteria are employed:

a. The elemental compositions for pyrolysis oils are reported,
b. GC/MS data for the pyrolysis oils are available,
c. calorific values of the pyrolysis oils are reported.

A total of 10 literature sources were identified and together provide 21 sets of data, produced from various types of feedstock. Ingram *et al*. [39] report four sets of pyrolysis oils analyses produced from pine wood, pine bark, oak wood and oak bark using an auger reactor. Zheng [40] reports data for pyrolysis oil produced from maize stalk using an electrically heated fluidized bed pyrolyzer with sand as the bed material. In a similar setup, Zheng *et al*. [41] produce pyrolysis oil from cotton stalk. Zhang *et al*. [46] carry out pyrolytic upgradation of sawdust in a fluidized bed. A comparison of the corrosive properties of pyrolysis oil produced from rice husk, and emulsions of the same with diesel, is reported by Lu *et al*. [43]. In an investigation of improving the properties of pyrolysis oils, Scholze [44] provides an extensive analysis of four different pyrolysis oils produced from beech wood, mixed hardwood, *Eucalyptus* wood, and pine wood. Mullen *et al*. [47] give an analysis and comparison of three pyrolysis oils produced from barley-based substrates, and additional data by Mullen *et al.* [42] are reported for two pyrolysis oils produced from corn cobs and stover. Ateş & Işikdağ [38] evaluate the relationship between pyrolytic temperature for pyrolysis oils produced from wheat and oat straws, and provide the most extensive characterisation but exclude moisture data when reporting elemental compositions and heats of combustion. These data collectively are summarized in Table 2 with respect to the elemental analyses of pyrolysis oils and calorific values.

Ingram *et al*. [39] report methods used for HHV, moisture determination, and ash, but it is unclear whether the elemental analysis and HHV measurements are reported on a dry and ash-fee basis. The calorific values are however reported as lower heating values. Similarly, Zheng *et al*. [40] do not describe the procedures used to obtain calorific and elemental data and also report the calorific value as the lower heating value. Therefore, the elemental data summarized in Table 2 have been recalculated to remove the moisture contribution for these data and calorific data to the higher heating value. Zheng *et al*. [41] report on the accuracy of the calorimetry analysis and report the lower heating value and together with Mullen *et al*. [42,47] provide the elemental analysis on a moisture-free basis, while Ateş & Işıkdağ [38] also account for ash and moisture content. These data in Table 2 are therefore shown as is. Zhang *et al*. [46] do not provide information for calorimetry, and report water content obtained from the GC/MS analysis, at 66 %, which seems erroneous when considered together with the higher heating value being reported. Therefore, the calorific value and elemental analysis is taken as is. Lu *et al*. [43] do not describe

the elemental and calorific analyses employed. When moisture analysis is used to correct for these analyses, the calculate higher heating value improves from a MAE of $7.1\ \mathrm{MJ\ kg^{-1}}$ to $0.3\ \mathrm{MJ\ kg^{-1}}$.

Scholze [44] provides a thorough description of the analytical procedures employed. It is mentioned that elemental analysis has been reported on a dry basis, and Dulong's formula has been used to determine calorific values. Therefore, it is more appropriate in this case to compare the calculated HHV's with the predicted HHV's. In this case, the MAE ranges from $2.8\ \mathrm{MJ\ kg^{-1}}$ to $4.6\ \mathrm{MJ\ kg^{-1}}$ (not shown in Table 2). Boateng *et al*. [48] do not describe the elemental analysis method, and it is assumed that data reported is on a wet basis, since recalculating these values improves the MAE between reported and calculated HHV's from $1.8\ \mathrm{MJ\ kg^{-1}}$ to $1.7\ \mathrm{MJ\ kg^{-1}}$ for pyrolysis oil collected from 4 condensers, and from $4.2\ \mathrm{MJ\ kg^{-1}}$ to $0.1\ \mathrm{MJ\ kg^{-1}}$ for pyrolysis oil collected from the electrostatic precipitator (ESP).

The highest MAE for predicted elemental analysis of $21.7\ \%$ was obtained for distiller's dried grains with solubles (DDGS) [47], which also obtained one of the highest MAE's for the calculated HHV ($\mathrm{MAE} = 7.8\ \mathrm{MJ\ kg^{-1}}$) using the reported elemental analysis, as well as the highest MAE for the predicted HHV ($\mathrm{MAE} = 13.7\ \mathrm{MJ\ kg^{-1}}$). The high error for the predicted HHV is expected since only $4\ \%$ of the compounds present in the pyrolysis oil were characterised. However, a considerably low oxygen content is reported, which does not seem to correspond with the lower than expected measured HHV of $-32.9\ \mathrm{MJ\ kg^{-1}}$. The same elemental and calorific data for DDGS also does not seem to correspond with those data reported by [38] who obtained a similar HHV but report an oxygen content of $19.8\ \%$. Overall, the MAE's for the predicted HHV's lie within a range of $0.1\ \mathrm{MJ\ kg^{-1}}$ and $6.0\ \mathrm{MJ\ kg^{-1}}$ (excluding the data set for DDGS), while those for the predicted HHV's and $0.1\ \mathrm{MJ\ kg^{-1}}$ and $9.9\ \mathrm{MJ\ kg^{-1}}$. The average for these MAE's HHV's are $3.9\ \mathrm{MJ\ kg^{-1}}$ and $3.5\ \mathrm{MJ\ kg^{-1}}$, respectively, while the average MAE of $6.1\ \%$ is obtained for the full set of elemental analysis predictions.

These errors seem to be reasonable, considering that only $29\ \%$ of the pyrolysis oil compounds have been characterised on average. Deviations from linearity are typically observed when plotting cumulative mass data, especially if characterisation is limited, and may be one of the reasons for the errors obtained for the literature data of Table 2. This is best explained graphically as shown in Figure 4, where reliance on mass characterisation of less than $20\ \%$ (Figure 4, data set A) tends to over predict the elemental mass composition (Figure 4, endpoint A^*). Even at higher mass characterisation of between 40 % (data set B) and 60 % (data set C) it is still possible to make poor predictions. Only at high mass characterisations (endpoints D^* and E^*) do errors become negligible. An alternative would be to sort the compound-based mass fractions from smallest to largest, as this is seen to reduce errors made when using linear regression to predict elemental and calorific data, as was observed in most of the literature data presented in Table 2. This method is less accurate when limited characterisation is available in the first place. This method may also be used to identify possible mistakes in such data as well, especially where a high level of GC/MS characterisation has been completed. Figure 5 demonstrates the accuracy produced by the proposed method for the case of predicting elemental compositions for wheat straw-derived pyrolysis oil when 96 % of the mass has been characterised (Figure 5, left graph). The same result has not been obtained for pyrolysis oil produced from oats straw for which a similar level of characterisation of 95 % has been achieved (Figure 5, middle graph). Irrespective of whether the remaining 4.96 % is accounted for as either solely oxygen, solely hydrogen, or solely carbon, the resulting mass balance still does not confirm the results reported by Ateş & Işıkdağ[38]. If, however, the reported elemental compositions are adjusted by subtracting an equivalent mass that corresponds to a moisture content of 11.15 % (which is determined using an iterative process as no moisture data is available for the study), the discrepancy observed is minimised almost completely (Figure 5, right graph).

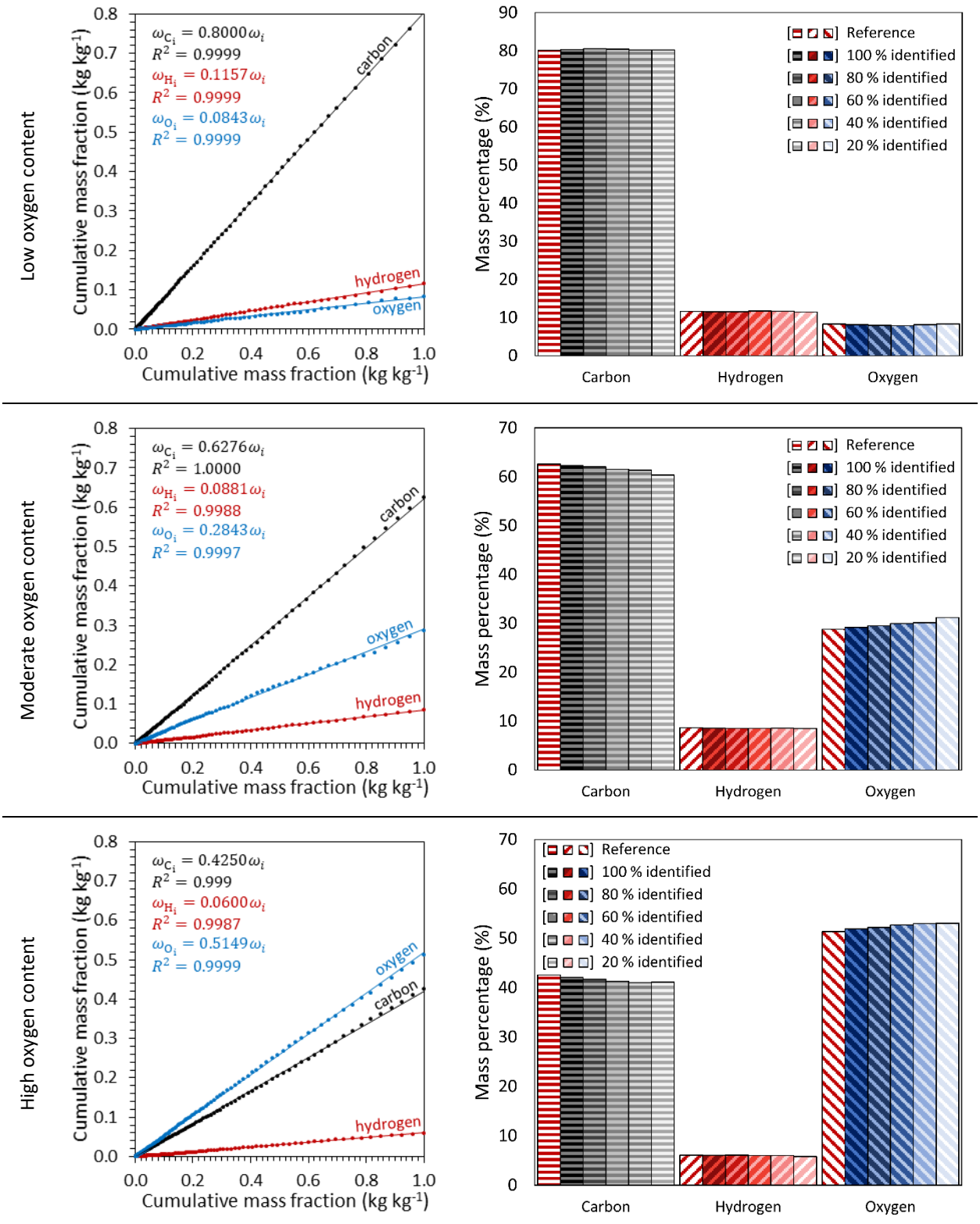

Figure 3: Plot of cumulative mass fractions of the elements against the total cumulative mass fraction (left); sensitivity analysis for predicting the mass percentages of elements C, H, and O using limited data (right).

The calculated data for the elemental composition of oats straw-derived pyrolysis oil ($\mathrm{C}\,\% = 74.4\,\%, \mathrm{H}\,\% = 8.1\,\%$ and $\mathrm{O}\,\% = 17.5\,\%$,) also compares more favourably with the elemental composition of wheat straw-derived pyrolysis oil ($\mathrm{C}\,\% = 71.1\,\%, \mathrm{H}\,\% = 8.5\,\%$ and $\mathrm{O}\,\% = 19.8\,\%$,). The corrected higher heating value obtained for oats straw-derived pyrolysis oil ($-32.0\ \mathrm{MJ\ kg^{-1}}$) is closer to wheat straw-derived pyrolysis oil ($-32.7\ \mathrm{MJ\ kg^{-1}}$) and the predicted value ($-34.0\ \mathrm{MJ\ kg^{-1}}$ and $\mathrm{MAE} = 1.9\ \mathrm{MJ\ kg^{-1}}$). Based on this analysis, it is possible that the reported elemental composition is presented on a wet basis rather than on the dray basis as stated.

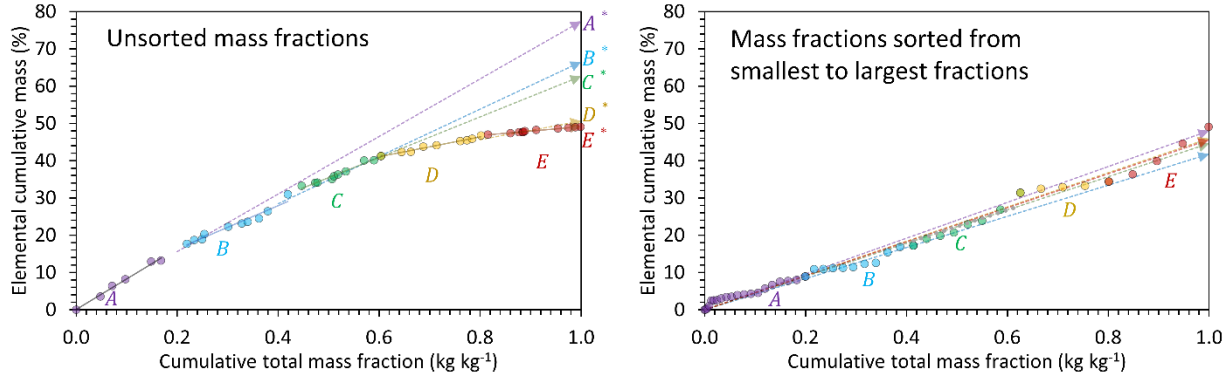

Figures 4: Effect of limited characterisation on accuracy of linear regression (left), and how sorting mass fractions from smallest to largest may improve efficacy of predicting elemental mass percentages (right).

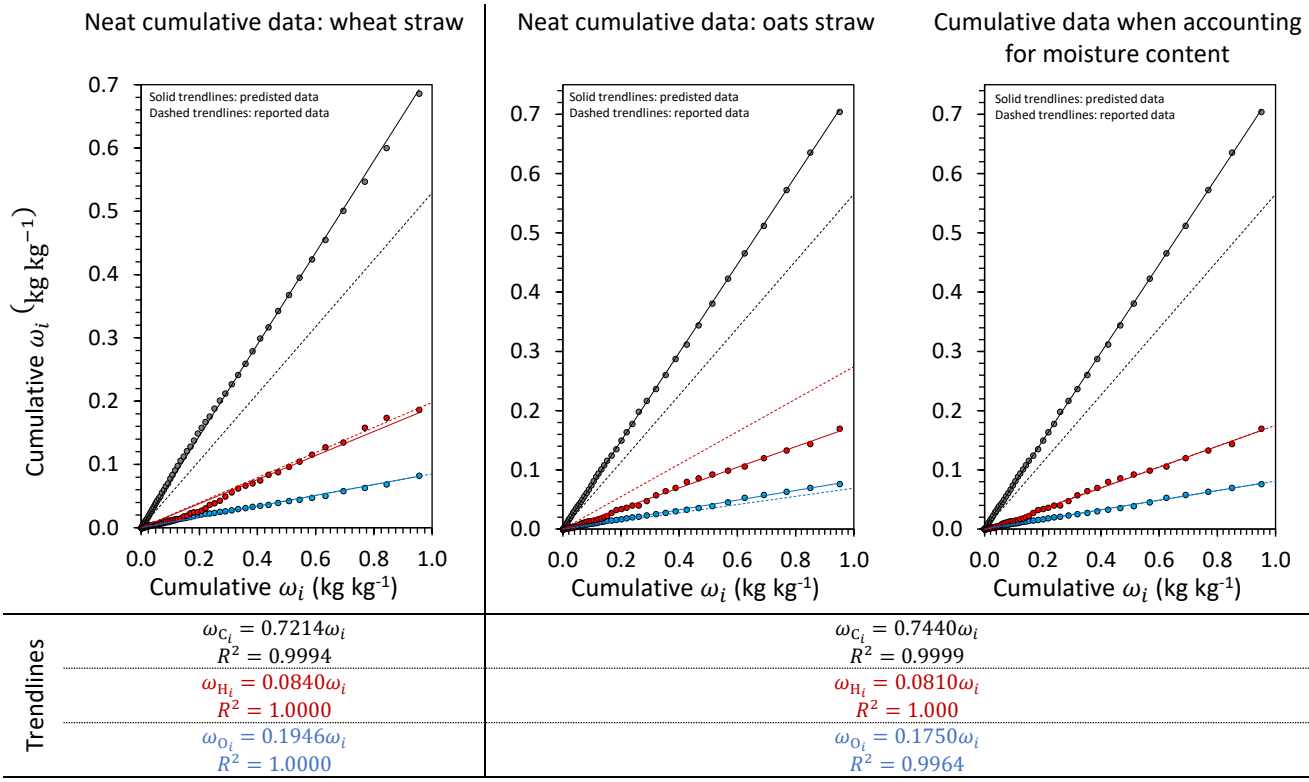

Figure 5: Plot of cumulative elemental mass percentages for carbon, hydrogen and oxygen against cumulative compound mass fractions for pyrolysis oil data for wheat straw and oats straw reported by Ateş & Işıkdağ[38]. These data show the accuracy obtained in predicting elemental compositions (left), as well as discrepancies that may arise due to mistakes in the data such as not accounting for moisture content when reporting elemental compositions (middle), and the increase in accuracy achieved when such mistakes have been corrected (right).

Table 2: Summary of elemental compositions and calorific values for fast pyrolysis oils obtained from the literature

Ref.	Feedstock	Compounds identified	Elemental mass reported[a] (%)					Elemental mass predicted (%)				HHV (MAE) ($\mathbf{MJ\ kg^{-1}}$)		
		%	C	H	O	N	S	C	H	O	MAE[b]	Reported[c]	Calculated[d]	Predicted[e]
[39]	Pine wood	28	52.6	7.5	39.5	0.1	0.0	59.5	6.3	34.2	4.4	−26.1	−22.3 (3.8)	−24.2 (1.9)
	Oak wood	35	47.2	4.5	50.0	0.1	0.0	56.3	6.3	37.4	7.8	−24.2	−15.2 (9.0)	−22.5 (1.6)
	Pine bark	31	54.0	7.0	38.2	0.4	0.0	51.9	6.3	51.9	2.2	−22.9	−22.5 (0.4)	−20.3 (2.7)
	Oak bark	18	45.5	6.1	47.8	0.3	0.3	60.7	6.4	32.9	10.1	−24.4	−17.0 (7.4)	−24.9 (0.5)
[40]	Maize stalk	23	58.6	5.0	36.4	0.6	0.3	57.7	7.5	34.8	1.7	−25.3	−22.1 (3.2)	−24.8 (0.5)
[41]	Cotton stalk	22	56.3	6.9	36.9	0.3	0.2	65.9	8.0	26.1	7.2	−23.5	−23.2 (0.3)	−29.6 (6.0)
[46]	Sawdust	34	60.4	6.9	41.8	0.9	0.0	51.1	7.7	41.1	3.6	−21.3	−22.1 (0.8)	−21.7 (0.4)
[43]	Rice husk	7	55.8	7.0	37.2	0.6	0.0	46.1	7.5	46.3	6.4	−22.8	−23.2 (0.3)	−18.9 (3.9)
[44]	Beech wood	23	51.7	7.5	40.5	0.4	0.0	48.2	6.8	45.0	2.9	−18.9	−21.8 (2.9)	−19.0 (0.1)
	Mixed hardwood	19	57.2	6.2	36.3	0.3	0.0	46.7	6.9	46.4	7.1	−13.1	−23.0 (9.9)	−18.4 (5.3)
	Eucalyptus wood	18	54.4	6.1	39.1	0.4	0.0	45.1	6.6	48.3	6.3	−15.0	−21.5 (6.5)	−17.2 (2.2)
	Pine wood	19	54.7	6.2	38.6	0.5	0.0	47.2	6.8	46.0	6.3	−16.2	−21.8 (5.6)	−18.6 (2.4)
[48]	Switchgrass - condenser	26	56.6	6.1	37.2	0.33	0.0	42.8	6.9	50.3	9.2	−20.8	−22.5 (1.7)	−16.5 (4.3)
	Switchgrass - ESP	14	57.4	6.2	36.4	0.38	0.0	44.0	6.5	49.5	8.9	−23.1	−23.0 (0.1)	−16.6 (6.6)
[42]	Corn cob	29	55.1	7.6	36.9	1.2	0.0	49.8	7.3	42.9	3.8	−26.2	−23.7 (2.5)	−20.5 (5.7)
	Corn stover	33	54.0	6.9	37.9	1.4	0.0	46.5	7.1	46.3	5.4	−24.3	−22.6 (1.7)	−18.6 (5.7)
[47]	Barley straw	19	50.8	3.2	44.4	1.8	0.0	49.5	7.5	43.0	2.3	−24.2	−16.4 (7.8)	−20.6 (3.6)
	Barley hulls	18	54.7	5.3	38.5	5.1	0.4	48.8	7.3	44.0	4.5	−24.1	−21.0 (3.1)	−19.9 (4.2)
	DDGS[f]	4	74.0	8.9	6.2	0.5	0.0	49.5	6.4	44.1	21.7	−32.9	−40.7 (7.8)	−19.2 (13.7)
[38]	Wheat straw	96	71.1	8.5	19.8	1.3	0.0	71.0	8.0	21.0	0.6	−32.7	−33.1 (0.4)	−32.2 (0.5)
	Oat straw	95	64.8	6.9	27.4	0.1	0.0	74.0	7.6	18.4	6.3	−27.1	−28.0 (0.9)	−33.1 (6.0)
	Averages:	29	56.5	6.5	36.5	0.8	0.1	53.0	7.0	40.5	6.1	−23.3	−23.2 (3.9)	−21.8 (3.5)

[a] As reported in the literature source. However, in some cases it appears that water content was not subtracted from the elemental analyses and produced MAE's that were considerably higher.

[b] The MAE shown here uses reported elemental compositions that are corrected for water content, and where it is suspected that elemental compositions have been reported without subtracting water content for the analyses, this is done to ensure consistency in these data.

[c] Values have been converted to a dry and ash-free basis where applicable.

[d] Calculated using the reported elemental analyses and Equation 8. In some cases, water has been removed from the reported elemental analysis reported, which led to improvements in these data.

[e] Using Equation 8.

[f] Distiller's dried grains with solubles.

3. Materials and method for the application of model to Py-GC/MS catalyst screening

3.1. Feedstock selection

The most important and abundant tree species grown for tropical and subtropical silviculture are from the *Eucalyptus* and *Pinus* genera, with their respective species contributing $26\ \%$ and $42\ \%$ of the total tree species internationally [49,50]. The *Eucalyptus* genus in particular is considered to comprise some of the fastest-growing species of trees compared to all other wood-type genera, based on rotation periods and mean annual increments [51,52]. The commercial importance of eucalypts has grown substantially over the past 60 years as a consequence of the superior fibre and pulping properties that they exhibit. It is their fast growth rates, shorter rotation periods and productivity that make eucalypts an attractive renewable source of biomass for energy production [53]. Not surprisingly, the thermal decomposition of *E. grandis* has been well researched. *E. grandis* has been used to evaluate property variations of torrefaction in an oxidative environment [54], and the catalytic conversion of its pyrolysis oil has also been reported [55]. Residues from *E. grandis* were therefore selected for investigating their suitability for producing pyrolysis oils, as well as for evaluating upgrading possibilities using the Py-GC/MS analytical method develop in this work. Four catalysts were considered for upgrading pyrolysis oils, namely ZSM-5 zeolite and bentonite as candidates for acid-based catalysis, and the Ca-Al and Mg-Al layered double oxides (LDO, derived from calcining their respective layered double hydroxides (LDH) [56]) as the alkali-based catalysis.

3.2. Feedstock preparation

E. grandis was sourced from Sappi Southern Africa as sawdust rejects with a maximum particle size of $6.0\ \mathrm{mm}$. This size was further reduced using a Retsch cutting mill, model SM 100, to obtain a particle size distribution between $150\ \mu\mathrm{m}$ and $250\ \mu\mathrm{m}$. Moisture was measured at $8.88\ \%$ using a Mettler Toledo Moisture Analyser LJ16.

3.3. Catalysts

ZSM-5 zeolite (sourced from Acros Organics) with a minimum surface area of $300\ \mathrm{m^2\ g^{-1}}$ (BET) and a $\mathrm{SiO_2}$: $\mathrm{Al_2O_3}$ molar ratio of between 400 and 570 was used as received. Bentonite clay was supplied in the form of a slurry ($19.2\ \%$ solids content, $\mathrm{pH}\ =\ 7.4$) by G&W Base and Industrial Minerals that was sourced from the Boane region in Mozambique. The cation exchange capacity was determined by the supplier to be $0.70\ \mathrm{meq\ g^{-1}}$ using the methylene blue method [57]. The bentonite slurry was centrifuged and washed using deionized water before being dried at $65\ ^{\circ}\mathrm{C}$. Ca-Al layered double hydroxide (LDH) was synthesised from CaO and $Al(OH)_3$ in a 2:1 molar ratio using an autoclave at 16 bar in an inert atmosphere of N_2. The reagents were first combined with degassed distilled water to form a slurry. The slurry was charged to the autoclave, mixed under high shear at 180 °C and allowed to cool gradually while mixing. Mg-Al LDH was synthesised using a similar process from the reagents MgO and $Al(OH)_3$ in a molar ratio of 2:1, albeit without the use of an inert atmosphere and in the presence of 1.6 times the stoichiometric amount of $NaHCO_3$. Both LDH products were filtered and washed repeatedly with distilled water to remove any unreacted reagents [58]. All catalysts were placed onto alumina supports to assist with catalysis: 10 % bentonite on alumina particles (*E. grandis* sample size of 1.231 mg), 10 % Ca-Al LDH on alumina particles (*E. grandis* sample size of 1.200 mg, where Ca-Al LDH converts to Ca-Al LDO during sintering > 700 °C[59]), 10 % Mg-Al LDH on alumina particles (*E. grandis* sample size of 1.100 mg, where Mg-Al LDH converts to Mg-Al LDO during sintering > 600 °C[60]), 10 % ZSM-5 on alumina particles (*E. grandis* sample sizes of 1.230 mg per temperature tested).

3.4. Methods and equipment

Pyrolysis oils were produced and characterized by pyrolysis-GC/MS (Py-GC/MS, Table 3) using a Shimadzu multi-functional pyrolyser EGA/PY-3030D from Frontier Laboratories, Japan. Evolved gas analysis (EGA-MS) was used to define the thermal desorption zone using a thermal programme of 100 °C to 600 °C at 20 °C min^{-1}. Sample sizes were in the range of 1.1 mg ± 0.1 mg. Samples are placed into small cups after which they free fall into the pyrolyser furnace and are heated to pyrolytic temperatures in less than 20 ms.

Table 3: Summary of operating conditions and parameters used for Py-GC/MS analysis

GC:	
Injection method:	1:50 split
Column:	polydimethylsiloxane, UA1: 30 m $\times$ 0.25 mm ID $\times$ 2 µm film thickness (2.0F) for pyrolysis at 500 °C, 30 m $\times$ 0.25 mm ID $\times$ 1 µm film thickness (1.0F) for pyrolysis at 300 °C
Flow rate:	Helium, 50 mL min^{-1}, 98 kPa
Temperature programming:	30 °C for 3 min, 20 °C min^{-1} to 350 °C, hold for 10 min
MS:	
Interface temperature:	300 °C
Ion trap temperature:	250 °C
Electron ionization (EI) scan range:	m/z 50 – 650

4. Results and discussion

4.1. Uncatalysed pyrolysis oil at 500 °C

The cumulative plots of Py-GC/MS data for pyrolysis oil produced from *E. grandis* shown near to linear regressions with respect to all elements (Figure 6). The predicted values for carbon ($62.4\ \% \pm 0.5\ \%$), hydrogen ($7.5\ \% \pm 0.5\ \%$), oxygen ($30.2\ \% \pm 0.0\ \%$), and calorific value ($\mathrm{HHV} = -27.1\ \mathrm{MJ\ kg^{-1}} \pm 0.5\ \mathrm{MJ\ kg^{-1}}$) (Table 4) differ only slightly from values for *E. grandis*-derived pyrolysis oil reported by Oasmaa *et al.* [7] (values corrected for moisture content: $\mathrm{C}\ \% = 53.3\ \%$, $\mathrm{H}\ \% = 6.6\ \%$ and $\mathrm{O}\ \% = 40.1\ \%$; $\mathrm{HHV} = -29.8\ \mathrm{MJ\ kg^{-1}}$) using a transport bed reactor, and Kim *et al.* [62] (values corrected for moisture content: $\mathrm{C}\ \% = 52.4\ \%$, $\mathrm{H}\ \% = 5.2\ \%$ and $\mathrm{O}\ \% = 42.4\ \%$; $\mathrm{HHV} = -25.3\ \mathrm{MJ\ kg^{-1}}$) using a fluidised bed reactor. Deviations between these sets of data are primarily due to corrections being made to the literature data coupled with the expected errors in analysis and the inefficiencies that arise from larger scale operations, compared to the more controlled synthesis and direct analysis obtained from Py-GC/MS.

The pyrogram produced from the pyrolysis of *E. grandis* via Py-GC/MS (Figure 7) shows the typical expected distribution of compounds derived from the degradation of lignin (represented by the aromatic compounds), cellulose and hemicellulose (represented by most of the non-aromatic compounds). The most prominent compounds identified are the aromatic compounds of 2,6-dimethoxy-phenol ($m_i = 5.5\ \%$), 1-(3,4-dimethoxyphenyl)-ethanone ($m_i = 3.9\ \%$), 2-methoxy-4-vinylphenol ($m_i = 3.5\ \%$), 2-methoxy-4-vinylphenol ($m_i = 3.5\ \%$) and 3-methoxy-1,2-benzenediol ($m_i = 3.4\ \%$), as well as cyclic compounds of 2-hydroxy-2-cyclopenten-1-one ($m_i = 3.8\ \%$), furfural ($m_i = 3.8\ \%$).

Table 4: Predicted physical data for uncatalyzed pyrolysis oil

Description	Elemental composition (%)				HHV $(\mathbf{MJ\ kg^{-1}})$
	C	H	O	Total	
Unsorted:	61.5	7.6	31.0	100.0	−26.8
Sorted, ascending:	63.1	7.7	29.2	100.0	−27.7
Sorted, descending:	62.6	7.1	30.3	100.0	−26.7
Averages:	**62.4**	**7.5**	**30.2**	**100.0**	**−27.1**
Standard errors:	**0.5**	**0.5**	**0.0**	**0.0**	**0.3**

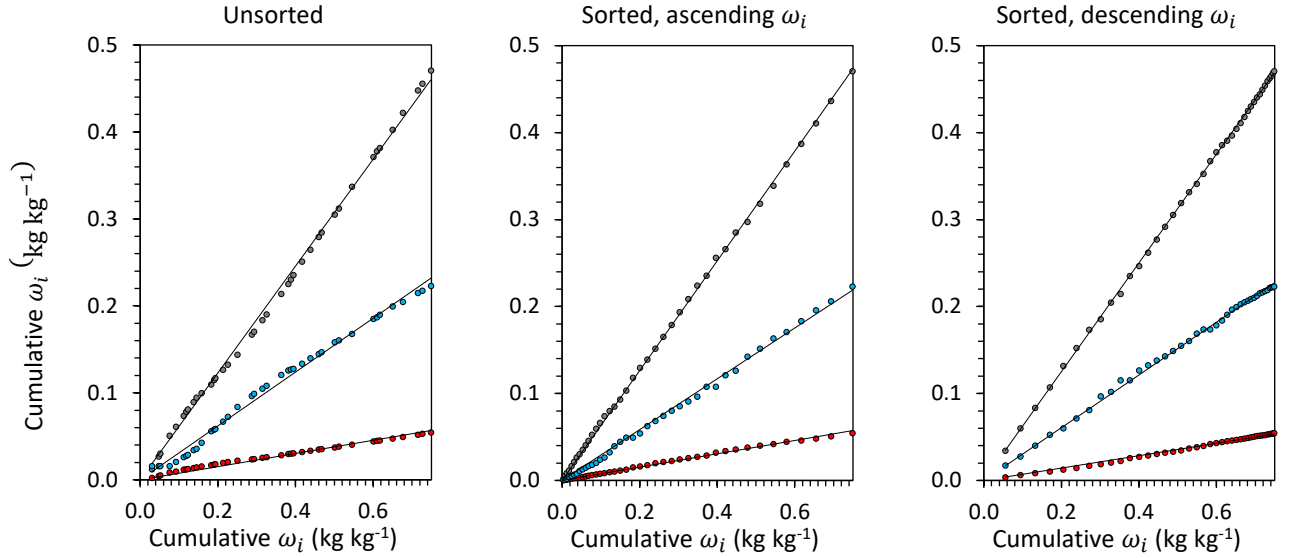

Trendlines			
	$\omega_{C_i} = 0.6146\omega_i$	$\omega_{C_i} = 0.63126\omega_i$	$\omega_{C_i} = 0.6256\omega_i$
	$R^2 = 0.9979$	$R^2 = 0.9996$	$R^2 = 0.9997$
	$\omega_{H_i} = 0.0758\omega_i$	$\omega_{H_i} = 0.0766\omega_i$	$\omega_{H_i} = 0.0712\omega_i$
	$R^2 = 0.9775$	$R^2 = 0.9964$	$R^2 = 0.9928$
	$\omega_{O_i} = 0.3097\omega_i$	$\omega_{O_i} = 0.2922\omega_i$	$\omega_{O_i} = 0.3032\omega_i$
	$R^2 = 0.9921$	$R^2 = 0.9974$	$R^2 = 0.9981$

Figure 6: Plot of cumulative elemental mass percentages for carbon, hydrogen and oxygen against cumulative compound mass fractions for uncatalyzed pyrolysis oil produced from *E. grandis* wood at 500 °C using Py-GC/MS.

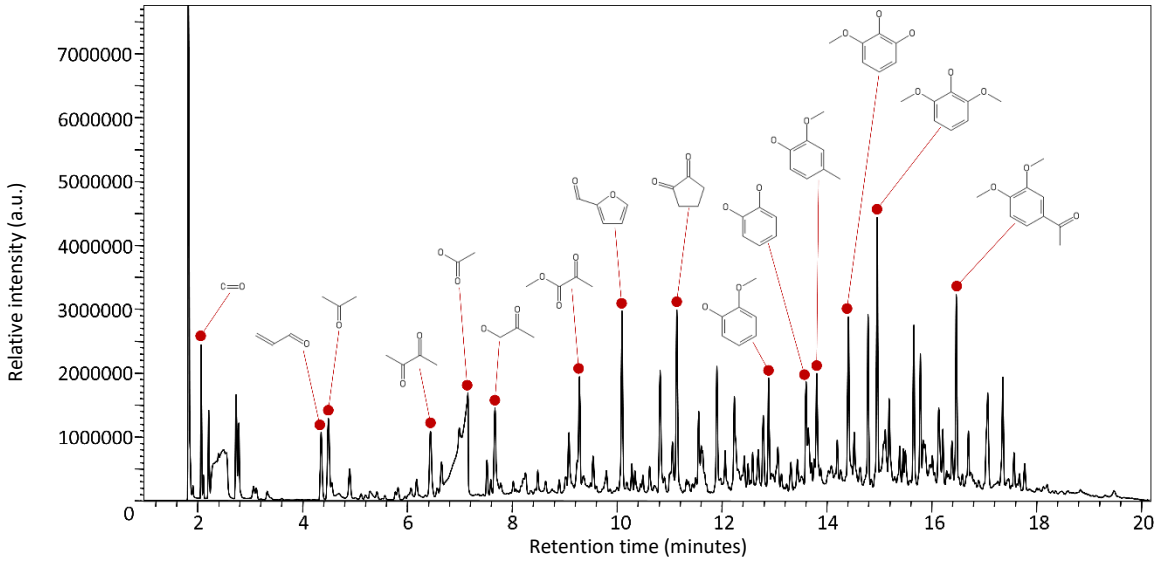

Figure 7: Pyrogram for products of uncatalyzed pyrolysis of *E. grandis* produced via Py-GC/MS

4.2. Bentonite-catalysed pyrolysis oil at 500 °C

Slight deviations from linearity for cumulative plots of Py-GC/MS data for bentonite-catalysed pyrolysis are observed, especially for oxygen content (Figure 8, middle and right graphs). Less pronounced deviations are also observed in the carbon trend (Figure 8, middle) and hydrogen trend (Figure 8, left). Those compounds with shorter residence time (where residence time corresponds with the consecutive order of unsorted data plotted in Figure 8), made up of non-aromatic compounds such as acetaldehyde ($m_i = 5.6\ \%$), formaldehyde ($m_i = 4.7\ \%$), methanol ($m_i = 3.7\ \%$), and acetone ($m_i = 3.4\ \%$), seem to have a slightly higher hydrogen content compared to those compounds with longer residence times, represented by mostly aromatic compounds such as 2,6-dimethoxyphenol ($m_i = 3.1\ \%$), 3,5-dimethoxyacetophenone ($m_i = 2.5\ \%$), and phenol ($m_i = 2.4\ \%$). This suggests that bentonite may be more active towards catalysing non-aromatic compounds. A slight increase in hydrogen (from $7.5\ \% \pm 0.5\ \%$ for uncatalyzed pyrolysis to $8.1\ \% \pm 0.6\ \%$ for bentonite-catalysed pyrolysis oil) and carbon (from $62.4\ \% \pm 0.5\ \%$ for uncatalyzed pyrolysis to $66.2\ \% \pm 0.7\ \%$ for bentonite-catalysed pyrolysis oil) is mostly due to a reduction in oxygen (from $30.2\ \% \pm 0.0\ \%$ for uncatalyzed pyrolysis to $25.7\ \% \pm 0.0\ \%$ for bentonite-catalysed pyrolysis oil) (Table 5). On a molar basis, the difference in chemical composition between uncatalyzed and bentonite-catalyse pyrolysis oils can be expressed by the following reaction equation:

$$C_{1.00}H_{1.42}O_{0.36} \rightarrow 0.95C_{1.00}H_{1.46}O_{0.29} + 0.05CO_2 + 0.04H_2O$$

where the ratio of water to carbon dioxide is 0.82. This indicates that bentonite-catalysed deoxygenation occurs through both the mechanisms of dehydration and decarboxylation with decarboxylation being slightly more dominant. The pyrogram for pyrolysis products produced from *E. grandis* in the presence of bentonite (Figure 9) shows a similar array of compounds to that of Figure 7.

Table 5: Predicted physical data for bentonite-catalyzed pyrolysis oil

Description	Elemental composition (%)				HHV $(\mathbf{MJ\ kg^{-1}})$
	C	**H**	**O**	**Total**	
Unsorted:	65.1	8.6	26.3	100.0	−29.8
Sorted, ascending:	67.6	7.8	24.6	100.0	−30.1
Sorted, descending:	65.8	7.8	26.3	100.0	−29.4
Averages:	**66.2**	**8.1**	**25.7**	**100.0**	**−29.8**
Standard errors:	**0.7**	**0.6**	**0.0**	**0.0**	**0.2**

4.3. ZSM-5-catalysed pyrolysis oil at 500 °C and 300 °C

Pyrolysis oil produced in the presence of ZSM-5 at 500 °C showed little to no catalytic activity (Table 6, Figure 10 and Figure 11) and achieved almost no upgrading in terms of deoxygenation. Only when using a lower temperature of 300 °C is catalysis via deoxygenation observed (Figure 12 and Figure 13). Very pronounced regions of catalysis are observed in Figure 12, where deoxygenation is obvious from the sudden reduction in the gradient for the oxygen trend (Figure 12, left) that accompanies a prominent increase in the carbon gradient and only a slight decrease in the hydrogen gradient. Considering these occurrences together with the equivalent chemical reaction formula of

$$C_{1.00}H_{1.42}O_{0.36} \rightarrow 0.97C_{1.00}H_{1.35}O_{0.22} + 0.033CO_2 + 0.117H_2O$$

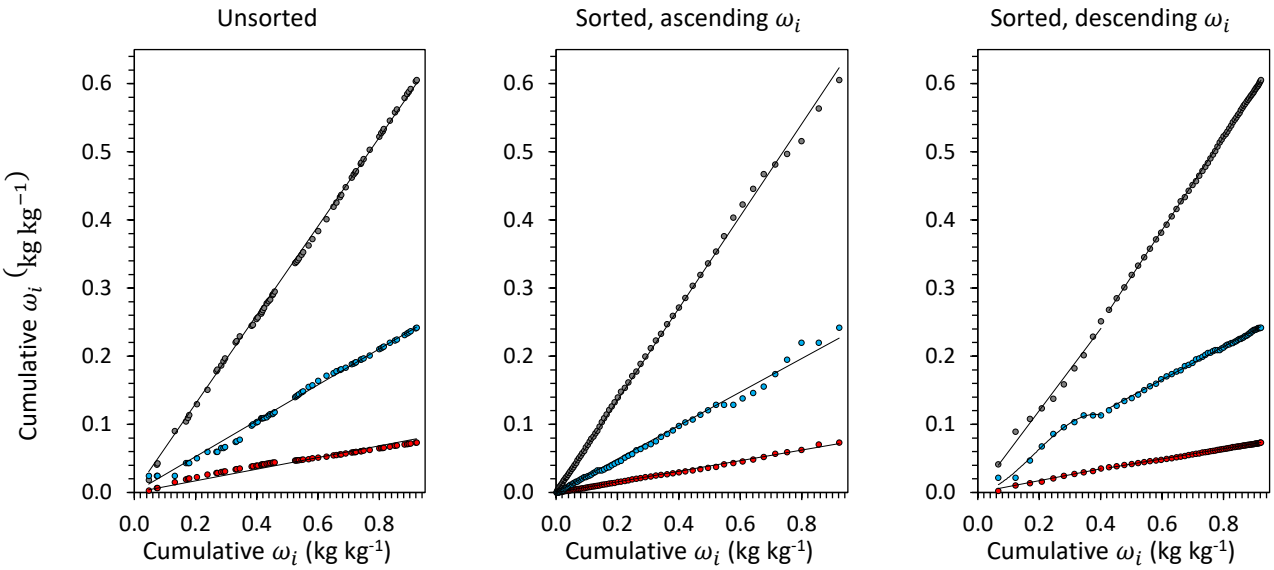

Trendlines	Unsorted	Sorted, ascending ω_i	Sorted, descending ω_i
	$\omega_{C_i} = 0.6512\omega_i$ $R^2 = 0.9992$	$\omega_{C_i} = 0.6763\omega_i$ $R^2 = 0.9987$	$\omega_{C_i} = 0.6829\omega_i - 0.0246$ $R^2 = 0.9998$
	$\omega_{H_i} = 0.0855\omega_i$ $R^2 = 0.9378$	$\omega_{H_i} = 0.0778\omega_i$ $R^2 = 0.9976$	$\omega_{H_i} = 0.0749\omega_i + 0.0043$ $R^2 = 0.9988$
	$\omega_{O_i} = 0.2633\omega_i$ $R^2 = 0.9941$	$\omega_{O_i} = 0.2458\omega_i$ $R^2 = 0.9923$	$\omega_{O_i} = 0.2422\omega_i + 0.0203$ $R^2 = 0.9980$

Figure 8: Plot of cumulative elemental mass percentages for carbon, hydrogen and oxygen against cumulative compound mass fractions for bentonite-catalyzed pyrolysis oil produced from *E. grandis* wood at 500 °C using Py-GC/MS.

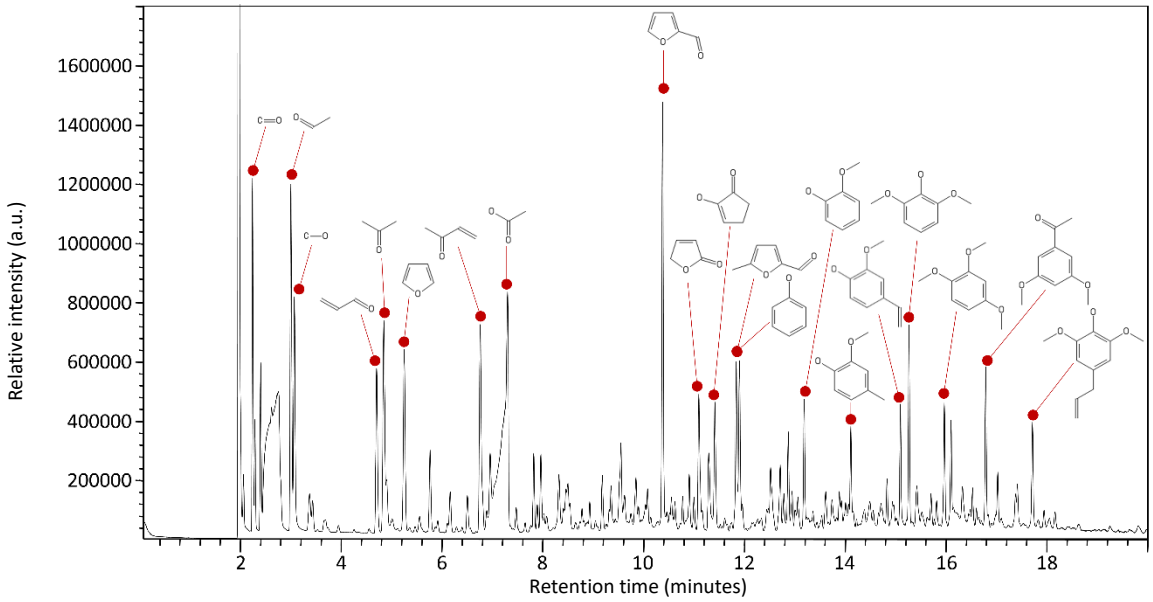

Figure 9: Pyrogram for products of bentonite-catalysed pyrolysis of *E. grandis* produced via Py-GC/MS

it is clear that with a ratio of water to carbon dioxide of 3.55, ZSM-5 achieves catalytic deoxygenation via dehydration and decarboxylation, where dehydration is the dominant mechanism. This produces a pyrolysis oil with a calorific value of $\mathrm{HHV} = -32.5\ \mathrm{MJ\ kg^{-1}} \pm 0.4\ \mathrm{MJ\ kg^{-1}}$ (Table 7). Even though deoxygenation relies heavily on dehydration, carbon dioxide as a leaving group is much heavier compared to water, and decarboxylation is still able to increase both carbon ($71.7\ \% \pm 1.3\ \%$) and hydrogen content ($8.1\ \% \pm 0.7\ \%$) of the pyrolysis oil, while reducing oxygen content down to $20.6\ \% \pm 0.0\ \%$.

Opposite to bentonite-catalysed pyrolysis, ZSM-5-catalysed pyrolysis impacts compounds with longer residence time (see unsorted data of Figure 12), made up of mostly lignin-derived aromatic compounds such as 1-methyl-4-(1-propynyl)-benzene ($m_i = 3.9\ \%$), toluene ($m_i = 3.5\ \%$), 2,3-dimethyl-1H-indene ($m_i = 3.4\ \%$), and 1,2-diphenyl-3-buten-1-ol ($m_i = 3.4\ \%$), and shows just about no activity for non-aromatic compounds (since the initial gradients for the unsorted data trendlines of Figure 12 are similar to those of uncatalyzed pyrolysis oil). This suggests that ZSM-5 catalysis at 300 °C is either biased towards the conversion of cellulosic derivatives to aromatic compounds or it may have limited catalytic potential on saccharide-derived pyrolysis oil fractions. As shown by the pyrogram of Figure 13, a reduced variety of compounds is produced as a result of this catalysis, and most aromatic compounds have also undergone deoxygenation compared to non-catalysed pyrolysis. The majority of studies with ZSM-5 have concluded that this catalyst gives the highest yield of (cellulosic derived) aromatics[63].

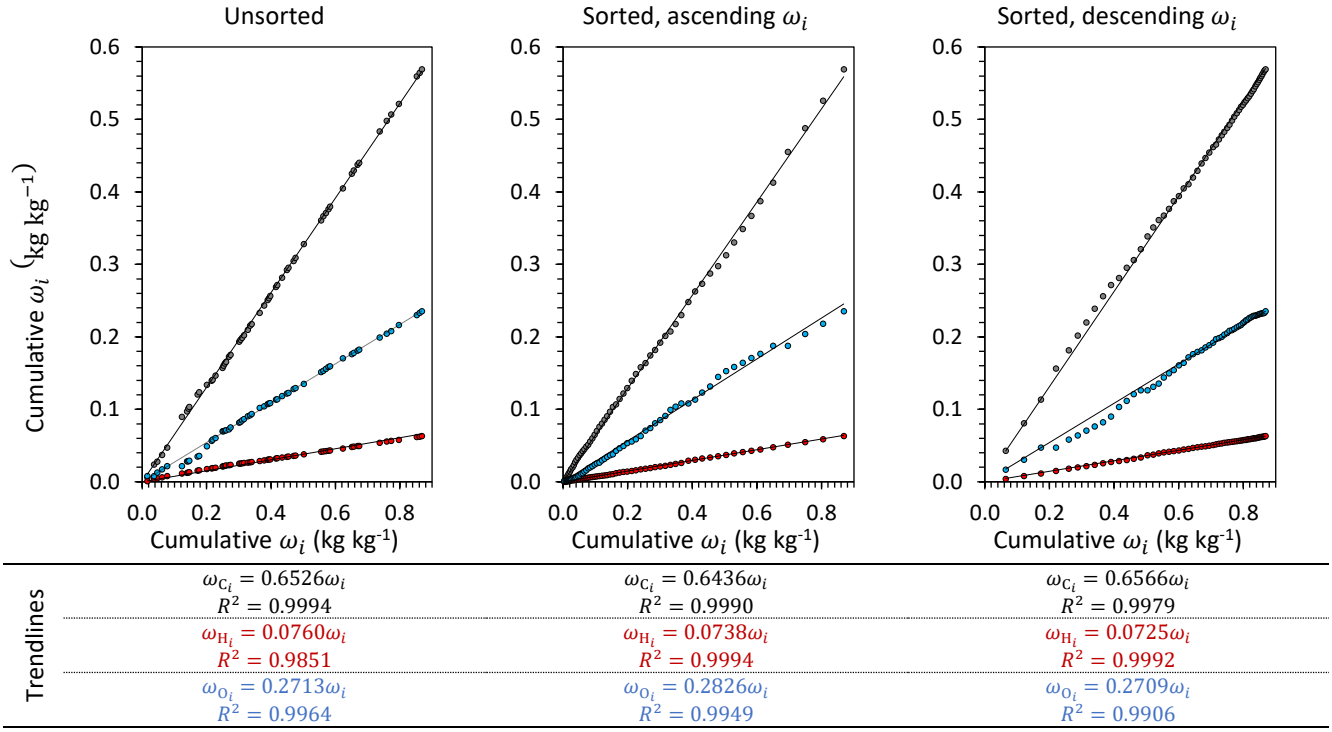

Trendlines			
	$\omega_{C_i} = 0.6526\omega_i$ $R^2 = 0.9994$	$\omega_{C_i} = 0.6436\omega_i$ $R^2 = 0.9990$	$\omega_{C_i} = 0.6566\omega_i$ $R^2 = 0.9979$
	$\omega_{H_i} = 0.0760\omega_i$ $R^2 = 0.9851$	$\omega_{H_i} = 0.0738\omega_i$ $R^2 = 0.9994$	$\omega_{H_i} = 0.0725\omega_i$ $R^2 = 0.9992$
	$\omega_{O_i} = 0.2713\omega_i$ $R^2 = 0.9964$	$\omega_{O_i} = 0.2826\omega_i$ $R^2 = 0.9949$	$\omega_{O_i} = 0.2709\omega_i$ $R^2 = 0.9906$

Figure 10: Plot of cumulative elemental mass percentages for carbon, hydrogen and oxygen against cumulative compound mass fractions for ZSM-5-catalyzed pyrolysis oil produced from *E. grandis* wood at 500 °C using Py-GC/MS.

A comparison of the initial gradients for carbon ($\mathrm{grad} = 0.5225$), hydrogen ($\mathrm{grad} = 0.0907$) and oxygen ($\mathrm{grad} = 0.3868$) of the ZSM-5-catalysed pyrolysis oil with the gradients of the uncatalyzed pyrolysis oil (Figure 6, middle: carbon ($\mathrm{grad} = 0.6312$), hydrogen ($\mathrm{grad} = 0.0766$) and oxygen ($\mathrm{grad} = 0.2922$)) show a reduction in carbon with an increase in both hydrogen and oxygen. This suggests that ZSM-5 does exhibit catalytic activity for non-aromatic compounds.

Table 6: Predicted physical data for pyrolysis oil produced in the presence of ZSM-5 at 500 °C

Description	Elemental composition (%)				HHV $(\mathbf{MJ\ kg^{-1}})$
	C	H	O	Total	
Unsorted:	65.3	7.6	27.1	100.0	-28.7
Sorted, ascending:	64.4	7.4	28.3	100.0	-28.0
Sorted, descending:	65.7	7.3	27.1	100.0	-28.5
Averages:	**65.1**	**7.4**	**27.5**	**100.0**	**-28.4**
Standard errors:	**0.4**	**0.4**	**0.0**	**0.0**	**0.2**

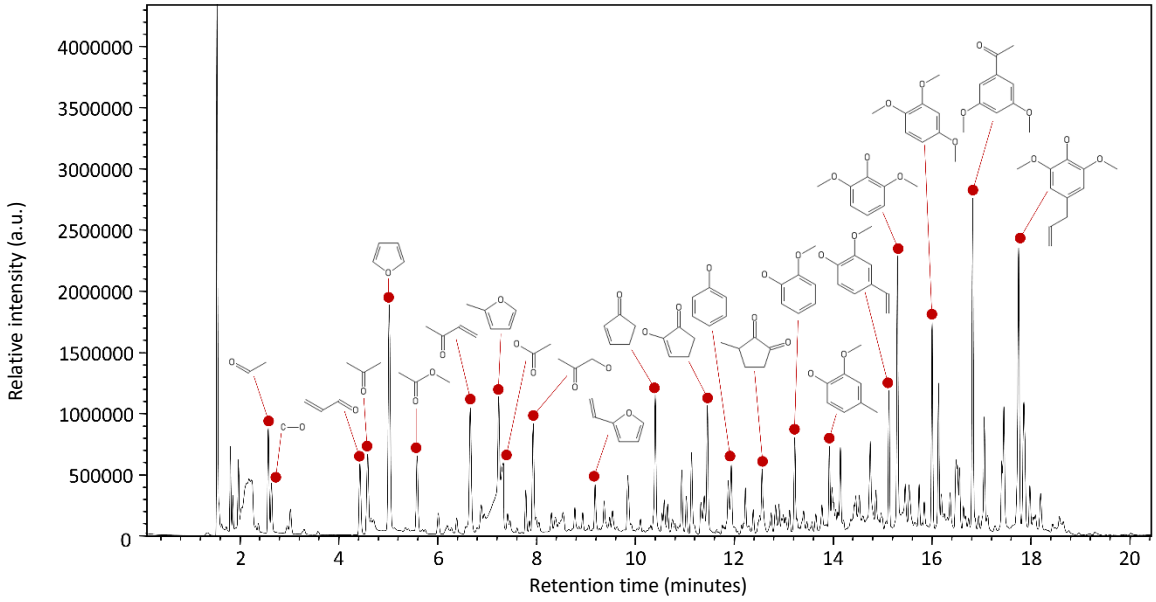

Figure 11: Pyrogram for pyrolysis of *E. grandis* in the presence of ZSM-5 produced via Py-GC/MS at 500 °C

Table 7: Predicted physical data for ZSM-5-catalysed pyrolysis oil produced at 300 °C

Description	Elemental composition (%)				HHV $(\mathbf{MJ\ kg^{-1}})$
	C	H	O	Total	
Unsorted:	71.4	8.1	20.5	100.0	-32.5
Sorted, ascending:	69.7	8.1	21.8	99.5	-31.8
Sorted, descending:	70.0	8.2	19.5	101.6	-33.1
Averages:	**71.7**	**8.1**	**20.6**	**100.4**	**-32.5**
Standard errors:	**1.3**	**0.7**	**0.0**	**0.0**	**0.4**

4.4. Ca-Al-LDO-catalysed and Mg-AL-catalysed pyrolysis oils at 500 °C

Pyrolysis oil catalysed with Ca-Al-LDO produced similar results as bentonite-catalysed pyrolysis oil in terms of overall trends observed in the plotted data (Figure 14 and Figure 15), elemental composition (at $\mathrm{C} = 64.2\ \% \pm 0.2\ \%$, $\mathrm{H} = 8.1\ \% \pm 0.5\ \%$ and $\mathrm{O} = 26.7\ \% \pm 0.0\ \%$ according to Table 8) and calorific value ($\mathrm{HHV} = -29.2\ \mathrm{MJ\ kg^{-1}}$), and follows upgradation (in reference to uncatalyzed pyrolysis oil) following the reaction equation of

$$\mathrm{C_{1.00}H_{1.42}O_{0.36}} \rightarrow 0.97\mathrm{C_{1.00}H_{1.51}O_{0.31}} + 0.065\mathrm{CO_2} + 0.011\mathrm{H_2O}$$

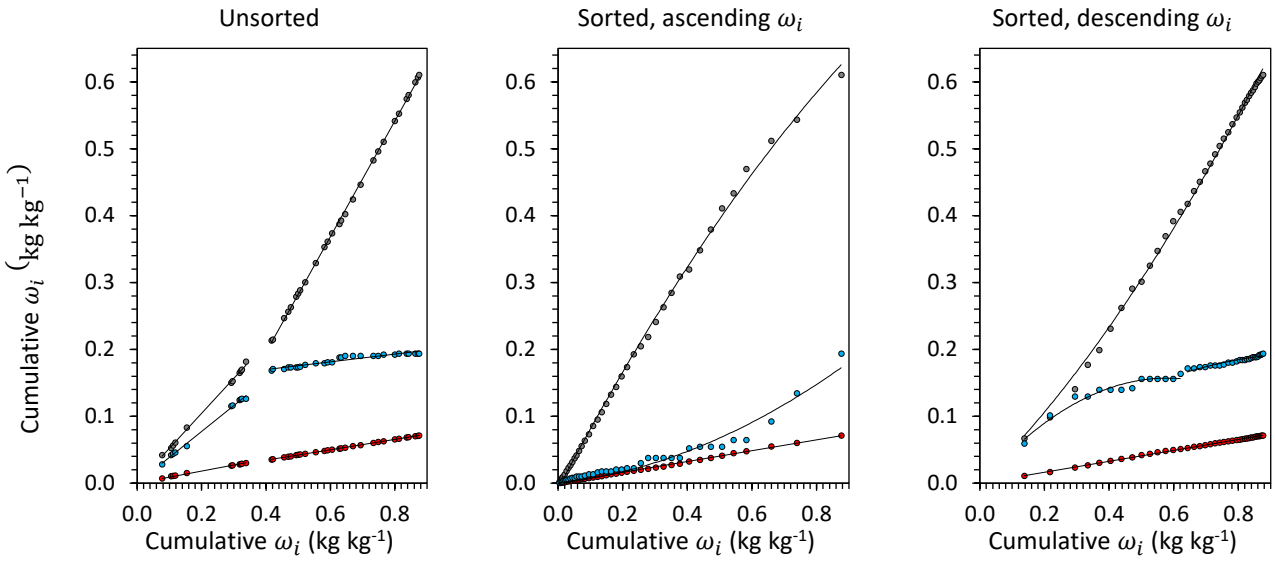

	Unsorted	Sorted, ascending ω_i	Sorted, descending ω_i
Trendlines	$\omega_{C_i} = 0.8643\omega_i - 0.1499$ $R^2 = 0.9996$	$\omega_{C_i} = -0.219\omega_i^2 + 0.9156\omega_i$ $R^2 = 0.9986$	$\omega_{C_i} = 0.2605\omega_i^2 + 0.4792\omega_i$ $R^2 = 0.9979$
	$\omega_{H_i} = 0.0778\omega_i + 0.0033$ $R^2 = 0.9996$	$\omega_{H_i} = 0.0810\omega_i$ $R^2 = 0.9991$	$\omega_{H_i} = 0.0817\omega_i$ $R^2 = 0.9988$
	$\omega_{O_i} = 0.0579\omega_i + 0.1467$ $R^2 = 0.9129$	$\omega_{O_i} = 0.1645\omega_i^2 + 0.0530\omega_i$ $R^2 = 0.9560$	$\omega_{O_i} = -0.1797\omega_i^2 + 0.3745\omega_i$ $R^2 = 0.9078$

Figure 12: Plot of cumulative elemental mass percentages for carbon, hydrogen and oxygen against cumulative compound mass fractions for ZSM-5-catalyzed pyrolysis oil produced from *E. grandis* wood at 300 °C using Py-GC/MS.

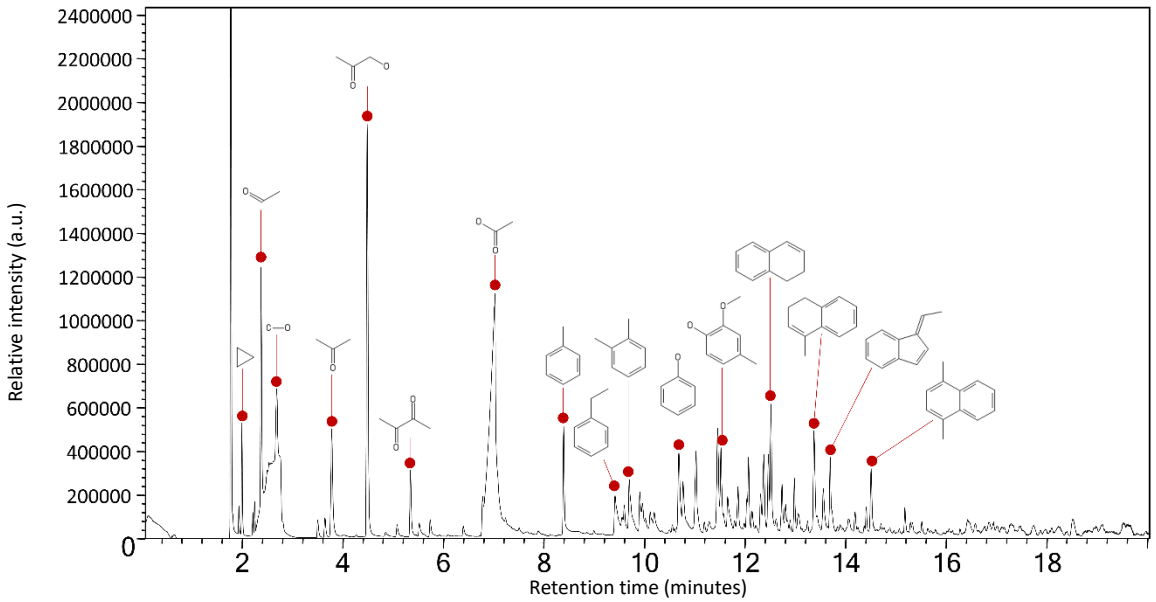

Figure 13: Pyrogram for products of ZSM-5-catalysed pyrolysis of *E. grandis* produced via Py-GC/MS

where decarboxylation is much more dominant that dehydration, with a ratio of water to decarboxylation of 0.18. This results in an increase in hydrogen content in the pyrolysis oil and a reduction in oxygen content. Since for every 2 moles of oxygen reporting to CO_2 for every mole of carbon, there is still a slight increase in carbon content as well (Table 8).

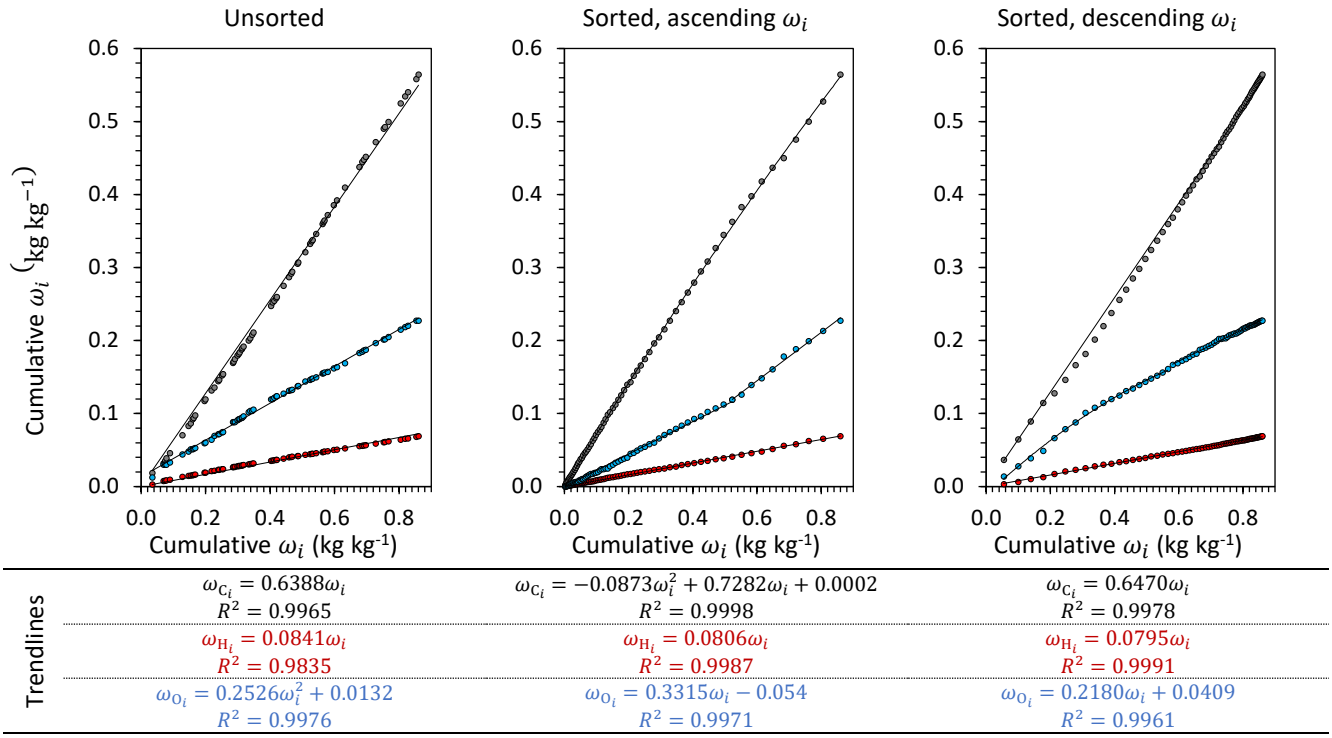

Trendlines			
	$\omega_{C_i} = 0.6388\omega_i$ $R^2 = 0.9965$	$\omega_{C_i} = -0.0873\omega_i^2 + 0.7282\omega_i + 0.0002$ $R^2 = 0.9998$	$\omega_{C_i} = 0.6470\omega_i$ $R^2 = 0.9978$
	$\omega_{H_i} = 0.0841\omega_i$ $R^2 = 0.9835$	$\omega_{H_i} = 0.0806\omega_i$ $R^2 = 0.9987$	$\omega_{H_i} = 0.0795\omega_i$ $R^2 = 0.9991$
	$\omega_{O_i} = 0.2526\omega_i^2 + 0.0132$ $R^2 = 0.9976$	$\omega_{O_i} = 0.3315\omega_i - 0.054$ $R^2 = 0.9971$	$\omega_{O_i} = 0.2180\omega_i + 0.0409$ $R^2 = 0.9961$

Figure 14: Plot of cumulative elemental mass percentages for carbon, hydrogen and oxygen against cumulative compound mass fractions for Ca-Al-LDO-catalyzed pyrolysis oil produced from *E. grandis* wood at 500 °C using Py-GC/MS.

Table 8: Predicted physical data for pyrolysis oil catalysed with Ca-Al-LDO at 500 °C

Description	**Elemental composition (%)**				**HHV (MJ kg^{-1})**
	C	**H**	**O**	**Total**	
Unsorted:	63.9	8.4	26.6	98.9	-29.5
Sorted, ascending:	64.1	8.1	27.8	99.9	-28.7
Sorted, descending:	64.7	8.0	25.9	98.5	-29.5
Averages:	**64.2**	**8.1**	**26.7**	**99.1**	**-29.2**
Standard errors:	**0.2**	**0.5**	**0.0**	**0.0**	**0.3**

Mg-Al-LDO achieves the highest deoxygenation of all catalysts investigated, which is observed by a strong decrease in the gradient for the oxygen data trend of Figure 16. Oxygen content is reduced to $12.7\,\% \pm 0.2\,\%$ while carbon and hydrogen content are increased to $77.3\,\% \pm 0.6\,\%$ and $9.3\,\% \pm 0.1\,\%$, respectively, and corresponds to a calorific value of $\mathrm{HHV} = -37.3\ \mathrm{MJ\ kg^{-1}} \pm 0.2\ \mathrm{MJ\ kg^{-1}}$ (Table 9). Compared with Ca-Al-LDO catalysis, Mg-Al-LDO catalysis seems to be dominated more by dehydration, which is 1.29 times that of decarboxylation, but deoxygenation overall is far more pronounced, and follows the reaction equation of

$$\mathrm{C_{1.00}H_{1.42}O_{0.36}} \rightarrow 0.89\mathrm{C_{1.00}H_{1.44}O_{0.12}} + 0.110\mathrm{CO_2} + 0.142\mathrm{H_2O}$$

This suggests that Mg-Al-LDO may be a harsher route for catalytic fast pyrolysis, and more investigations into the effects of temperature should be completed to determine whether the ratio of dehydration and decarboxylation may be altered to achieve deoxygenation primarily through the routes of decarboxylation

or decarbonylation. The effect of the mode of deoxygenation is obvious from the significant reduction in the distribution of compounds present in the pyrogram of Figure 17, where most of the saccharide-derived pyrolysis products have been reduced and the remaining compounds are mostly deoxygenated lignin-derived (or possibly saccharide-derived) aromatics.

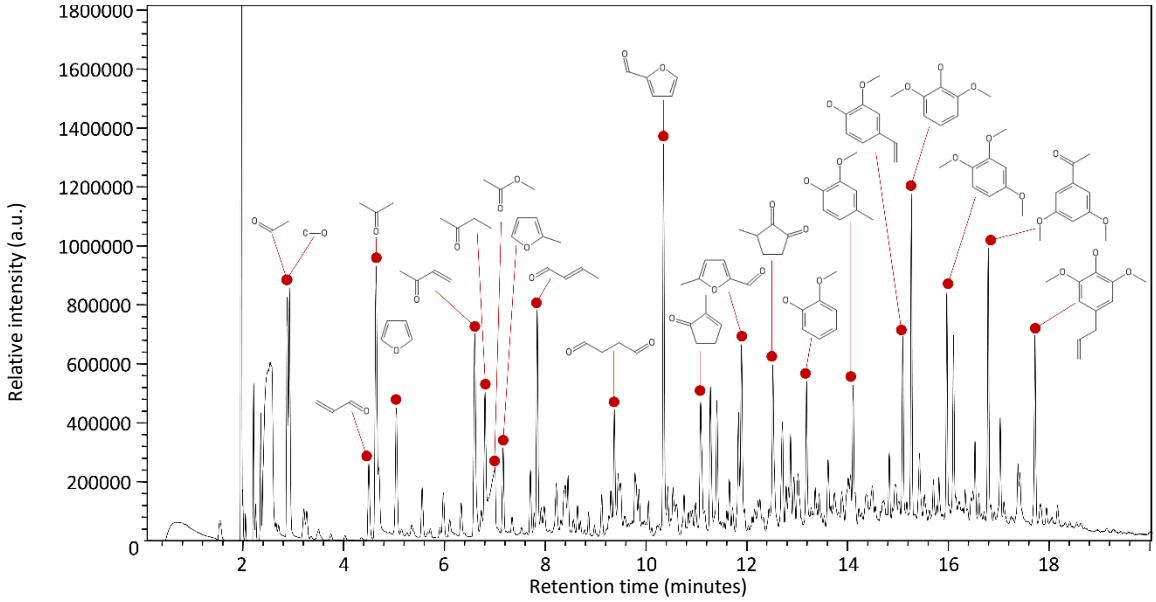

Figure 15: Pyrogram for products of Ca-Al LDO-catalysed pyrolysis of *E. grandis* produced via Py-GC/MS

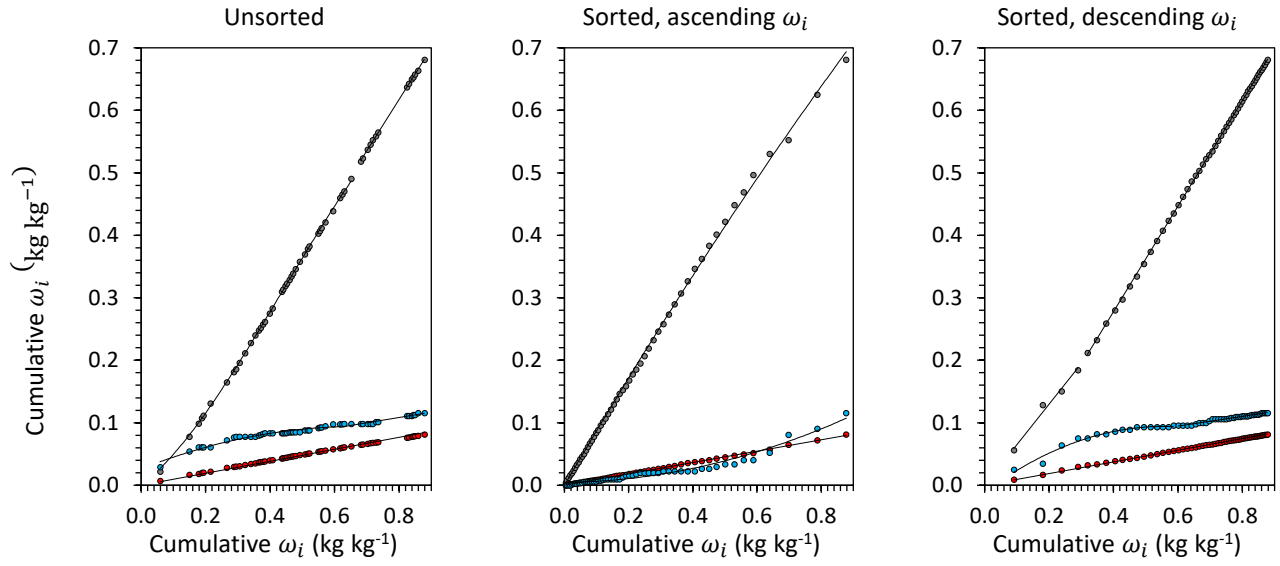

Trendlines	Unsorted	Sorted, ascending ω_i	Sorted, descending ω_i
	$\omega_{C_i} = 0.8191\omega_i - 0.0381$ $R^2 = 0.9997$	$\omega_{C_i} = -0.1018\omega_i^2 + 0.8792\omega_i$ $R^2 = 0.9991$	$\omega_{C_i} = 0.8444\omega_i - 0.06$ $R^2 = 0.9999$
	$\omega_{H_i} = 0.0959\omega_i$ $R^2 = 0.9917$	$\omega_{H_i} = 0.0909\omega_i$ $R^2 = 0.9993$	$\omega_{H_i} = 0.0934\omega_i$ $R^2 = 0.9984$
	$\omega_{O_i} = 0.0848\omega_i + 0.0406$ $R^2 = 0.9312$	$\omega_{O_i} = 0.099\omega_i^2 + 0.0315\omega_i$ $R^2 = 0.9488$	$\omega_{O_i} = 0.0779\omega_i + 0.0479$ $R^2 = 0.9759$

Figure 16: Plot of cumulative elemental mass percentages for carbon, hydrogen and oxygen against cumulative compound mass fractions for Mg-Al-LDO-catalyzed pyrolysis oil produced from *E. grandis* wood at 500 °C using Py-GC/MS.

Table 9: Predicted physical data for pyrolysis oil catalysed with Mg-Al-LDO at 500 °C

Description	Elemental composition (%)				HHV $(\mathbf{MJ\ kg^{-1}})$
	C	H	O	Total	
Unsorted:	78.1	9.6	12.5	100.2	-37.6
Sorted, ascending:	77.7	9.1	13.1	99.9	-37.0
Sorted, descending:	76.1	9.3	12.6	98.0	-37.4
Averages:	**77.3**	**9.3**	**12.7**	**99.4**	**-37.3**
Standard errors:	**0.6**	**0.1**	**0.2**	**0.0**	**0.2**

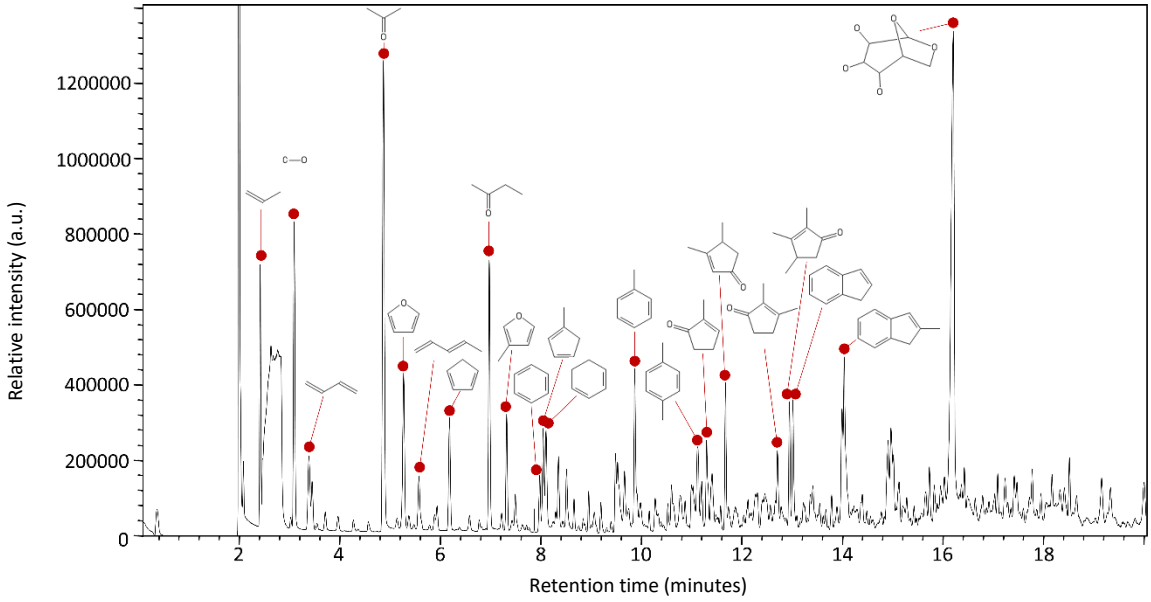

Figure 17: Pyrogram for products of Mg-Al LDO-catalysed pyrolysis of *E. grandis* produced via Py-GC/MS

5. Conclusions

The usefulness of Py-GC/MS as an analytical tool, coupled with the add-on ability to perform evolved gas analysis and thereby define the thermal desorption zone, is further enhanced by the new combined indirect method of analysis presented in this work. Such a method of analysis reduces the need for multiple analytical equipment when determining elemental composition, moisture content and heat of combustion for pyrolysis oils. The reliability of this method to predict the elemental compositions is validated using a large data set obtained from the literature (although most data was found to have a low average incident of characterisation of 29 %). It was also demonstrated that it is possible to use this method of analysis to confirm and correct for possible errors obtained from other analytical techniques. This shortcut method is further extended to assess the performance of various catalysts in upgrading pyrolysis oil produced from *E.* grandis sawdust. With uncatalyzed pyrolysis oil as reference ($\mathrm{HHV} = -27.1\ \mathrm{MJ\ kg^{-1}} \pm 0.3\ \mathrm{MJ\ kg^{-1}}$), catalytic performance between catalysts tested increased in order of ZSM-5 at 500 °C ($\mathrm{HHV} = -28.4\ \mathrm{MJ\ kg^{-1}} \pm 0.2\ \mathrm{MJ\ kg^{-1}}$), Ca-Al-LDO ($\mathrm{HHV} = -29.2\ \mathrm{MJ\ kg^{-1}} \pm 0.3\ \mathrm{MJ\ kg^{-1}}$), Bentonite ($\mathrm{HHV} = -29.8\ \mathrm{MJ\ kg^{-1}} \pm 0.2\ \mathrm{MJ\ kg^{-1}}$), ZSM-5 at 300 °C ($\mathrm{HHV} = -32.5\ \mathrm{MJ\ kg^{-1}} \pm 0.4\ \mathrm{MJ\ kg^{-1}}$), and Mg-Al-LDO ($\mathrm{HHV} = -37.3\ \mathrm{MJ\ kg^{-1}} \pm 0.2\ \mathrm{MJ\ kg^{-1}}$). Catalytic fast pyrolysis by Ca-Al-LDO was found to be strongly dominated by decarboxylation, with a dehydration to decarboxylation ratio of $\mathrm{H_2O/CO_2} = 0.18$, compared to Mg-Al-LDO ($\mathrm{H_2O/CO_2} = 1.29$) and bentonite ($\mathrm{H_2O/CO_2} = 0.82$), which was more balanced between dehydration and decarboxylation. ZSM-5 at 300 °C led to decarboxylation relying heavily on dehydration, with $\mathrm{H_2O/CO_2} = 3.55$.

6. Acknowledgements

The authors also acknowledge the continued financial support received from the Paper Manufacturers Association of South Africa (PAMSA).

7. References

[1] F.-X. Collard, J. Blin, A review on pyrolysis of biomass constituents: Mechanisms and composition of the products obtained from the conversion of cellulose, hemicelluloses and lignin, Renewable and Sustainable Energy Reviews. 38 (2014) 594–608. https://doi.org/10.1016/j.rser.2014.06.013.

[2] M.I. Jahirul, M.G. Rasul, A.A. Chowdhury, N. Ashwath, Biofuels Production through Biomass Pyrolysis —A Technological Review, Energies. 5 (2012) 4952–5001. https://doi.org/10.3390/en5124952.

[3] D. Mohan, C.U. Pittman, P.H. Steele, Pyrolysis of Wood/Biomass for Bio-oil: A Critical Review, Energy Fuels. 20 (2006) 848–889. https://doi.org/10.1021/ef0502397.

[4] A. Demirbas, The influence of temperature on the yields of compounds existing in bio-oils obtained from biomass samples via pyrolysis, Fuel Processing Technology. 88 (2007) 591–597. https://doi.org/10.1016/j.fuproc.2007.01.010.

[5] A.V. Bridgwater, Review of fast pyrolysis of biomass and product upgrading, Biomass and Bioenergy. 38 (2012) 68–94. https://doi.org/10.1016/j.biombioe.2011.01.048.

[6] J.P. Diebold, S. Czernik, Additives To Lower and Stabilize the Viscosity of Pyrolysis Oils during Storage, Energy Fuels. 11 (1997) 1081–1091. https://doi.org/10.1021/ef9700339.

[7] A. Oasmaa, E. Kuoppala, J.-F. Selin, S. Gust, Y. Solantausta, Fast Pyrolysis of Forestry Residue and Pine. 4. Improvement of the Product Quality by Solvent Addition, Energy Fuels. 18 (2004) 1578–1583. https://doi.org/10.1021/ef040038n.

[8] M. Ikura, M. Stanciulescu, E. Hogan, Emulsification of pyrolysis derived bio-oil in diesel fuel, Biomass and Bioenergy. 24 (2003) 221–232. https://doi.org/10.1016/S0961-9534(02)00131-9.

[9] D. Chiaramonti, M. Bonini, E. Fratini, G. Tondi, K. Gartner, A.V. Bridgwater, H.P. Grimm, I. Soldaini, A. Webster, P. Baglioni, Development of emulsions from biomass pyrolysis liquid and diesel and their use in engines—Part 1 : emulsion production, Biomass and Bioenergy. 25 (2003) 85–99. https://doi.org/10.1016/S0961-9534(02)00183-6.

[10] H.J. Park, J.-K. Jeon, D.J. Suh, Y.-W. Suh, H.S. Heo, Y.-K. Park, Catalytic Vapor Cracking for Improvement of Bio-Oil Quality, Catal Surv Asia. 15 (2011) 161–180. https://doi.org/10.1007/s10563-011-9119-7.

[11] J. Wildschut, I. Melián-Cabrera, H.J. Heeres, Catalyst studies on the hydrotreatment of fast pyrolysis oil, Applied Catalysis B: Environmental. 99 (2010) 298–306. https://doi.org/10.1016/j.apcatb.2010.06.036.

[12] X. Li, R. Gunawan, C. Lievens, Y. Wang, D. Mourant, S. Wang, H. Wu, M. Garcia-Perez, C.-Z. Li, Simultaneous catalytic esterification of carboxylic acids and acetalisation of aldehydes in a fast pyrolysis bio-oil from mallee biomass, Fuel. 90 (2011) 2530–2537. https://doi.org/10.1016/j.fuel.2011.03.025.

[13] M.M. Wright, R.C. Brown, A.A. Boateng, Distributed processing of biomass to bio-oil for subsequent production of Fischer-Tropsch liquids, Biofuels, Bioproducts and Biorefining. 2 (2008) 229–238. https://doi.org/10.1002/bbb.73.

[14] M.W. Nolte, B.H. Shanks, A Perspective on Catalytic Strategies for Deoxygenation in Biomass Pyrolysis, Energy Technology. 5 (2017) 7–18. https://doi.org/10.1002/ente.201600096.

[15] R.H. Venderbosch, A critical view on catalytic pyrolysis of biomass, ChemSusChem. 8 (2015) 1306–1316. https://doi.org/10.1002/cssc.201500115.

[16] S.R. Naqvi, Y. Uemura, S. Yusup, Y. Sugiur, N. Nishiyama, M. Naqvi, The Role of Zeolite Structure and Acidity in Catalytic Deoxygenation of Biomass Pyrolysis Vapors, Energy Procedia. 75 (2015) 793–800. https://doi.org/10.1016/j.egypro.2015.07.126.

[17] A. Zheng, Z. Zhao, S. Chang, Z. Huang, H. Wu, X. Wang, F. He, H. Li, Effect of crystal size of ZSM-5 on the aromatic yield and selectivity from catalytic fast pyrolysis of biomass, Journal of Molecular Catalysis A: Chemical. 383–384 (2014) 23–30. https://doi.org/10.1016/j.molcata.2013.11.005.

[18] X. Li, L. Su, Y. Wang, Y. Yu, C. Wang, X. Li, Z. Wang, Catalytic fast pyrolysis of Kraft lignin with HZSM-5 zeolite for producing aromatic hydrocarbons, Front. Environ. Sci. Eng. 6 (2012) 295–303. https://doi.org/10.1007/s11783-012-0410-2.

[19] Md.M. Rahman, R. Liu, J. Cai, Catalytic fast pyrolysis of biomass over zeolites for high quality bio-oil – A review, Fuel Processing Technology. 180 (2018) 32–46. https://doi.org/10.1016/j.fuproc.2018.08.002.

[20] B. Puértolas, Q. Imtiaz, C.R. Müller, J. Pérez-Ramírez, Platform Chemicals via Zeolite-Catalyzed Fast Pyrolysis of Glucose, ChemCatChem. 9 (2017) 1579–1582. https://doi.org/10.1002/cctc.201601052.

[21] G. Yildiz, F. Ronsse, R. van Duren, W. Prins, Challenges in the design and operation of processes for catalytic fast pyrolysis of woody biomass, Renewable and Sustainable Energy Reviews. 57 (2016) 1596–1610. https://doi.org/10.1016/j.rser.2015.12.202.

[22] T. Dickerson, J. Soria, Catalytic Fast Pyrolysis: A Review, Energies. 6 (2013) 514–538. https://doi.org/10.3390/en6010514.

[23] G. Yildiz, F. Ronsse, W. Prins, CHAPTER 10:Catalytic Fast Pyrolysis Over Zeolites, in: Fast Pyrolysis of Biomass, 2017: pp. 200–230. https://doi.org/10.1039/9781788010245-00200.

[24] Q. Lu, X. Yang, C. Dong, Z. Zhang, X. Zhang, X. Zhu, Influence of pyrolysis temperature and time on the cellulose fast pyrolysis products: Analytical Py-GC/MS study, Journal of Analytical and Applied Pyrolysis. 92 (2011) 430–438. https://doi.org/10.1016/j.jaap.2011.08.006.

[25] B. Zhang, Z. Zhong, K. Ding, Z. Song, Production of aromatic hydrocarbons from catalytic co-pyrolysis of biomass and high density polyethylene: Analytical Py–GC/MS study, Fuel. 139 (2015) 622–628. https://doi.org/10.1016/j.fuel.2014.09.052.

[26] C.A. Mullen, A.A. Boateng, Catalytic pyrolysis-GC/MS of lignin from several sources, Fuel Processing Technology. 91 (2010) 1446–1458. https://doi.org/10.1016/j.fuproc.2010.05.022.

[27] T. Ohra-aho, J. Linnekoski, Catalytic pyrolysis of lignin by using analytical pyrolysis-GC–MS, Journal of Analytical and Applied Pyrolysis. 113 (2015) 186–192. https://doi.org/10.1016/j.jaap.2014.12.012.

[28] Q. Lu, Z.-F. Zhang, C.-Q. Dong, X.-F. Zhu, Catalytic Upgrading of Biomass Fast Pyrolysis Vapors with Nano Metal Oxides: An Analytical Py-GC/MS Study, Energies. 3 (2010) 1805–1820. https://doi.org/10.3390/en3111805.

[29] J. Rodrigues, D. Meier, O. Faix, H. Pereira, Determination of tree to tree variation in syringyl/guaiacyl ratio of Eucalyptus globulus wood lignin by analytical pyrolysis, Journal of Analytical and Applied Pyrolysis. 48 (1999) 121–128. https://doi.org/10.1016/S0165-2370(98)00134-X.

[30] Q. Lu, Z. Zhang, X. Yang, C. Dong, X. Zhu, Catalytic fast pyrolysis of biomass impregnated with K3PO4 to produce phenolic compounds: Analytical Py-GC/MS study, Journal of Analytical and Applied Pyrolysis. 104 (2013) 139–145. https://doi.org/10.1016/j.jaap.2013.08.011.

[31] R.D. Merckel, F.J.W.J. Labuschagne, M.D. Heydenrych, Oxygen consumption as the definitive factor in predicting heat of combustion, Applied Energy. 235 (2019) 1041–1047. https://doi.org/10.1016/j.apenergy.2018.10.111.

[32] R. Merckel, F. Labuschagne, M. Heydenrych, Corrigendum to “Oxygen consumption as the definitive factor in predicting heat of combustion” [Appl. Energy 235 (2019) 1041-1047], 254 (2019) 1041–1047. https://doi.org/10.1016/j.apenergy.2019.113628.

[33] M. Staš, M. Auersvald, L. Kejla, D. Vrtiška, J. Kroufek, D. Kubička, Quantitative analysis of pyrolysis bio-oils: A review, TrAC Trends in Analytical Chemistry. 126 (2020) 115857. https://doi.org/10.1016/j.trac.2020.115857.

[34] O.D. Sparkman, Z. Penton, F.G. Kitson, Section 1: The Fudamentals of GC/MS, in: Gas Chromatography and Mass Spectrometry: A Practical Guide, Academic Press, 2011.

[35] R. Merckel, F. Labuschagne, M. Heydenrych, Oxygen as the definitive factor in predicting heat of combustion, Applied Energy. 235 (2019) 1041–1047. https://doi.org/10.1016/j.apenergy.2018.10.111.

[36] Perry’s Chemical Engineers’ Handbook, 9th Edition | McGraw-Hill Education - Access Engineering, (n.d.). https://www.accessengineeringlibrary.com/content/book/9780071834087 (accessed October 11, 2019).

[37] E.S. Domalski, Selected Values of Heats of Combustion and Heats of Formation of Organic Compounds Containing the Elements C, H, N, O, P, and S., Journal of Physical and Chemical Reference Data. 1 (1972) 221–277. https://doi.org/10.1063/1.3253099.

[38] F. Ateş, M.A. Işıkdağ, Evaluation of the Role of the Pyrolysis Temperature in Straw Biomass Samples and Characterization of the Oils by GC/MS, Energy Fuels. 22 (2008) 1936–1943. https://doi.org/10.1021/ef7006276.

[39] L. Ingram, D. Mohan, M. Bricka, P. Steele, D. Strobel, D. Crocker, B. Mitchell, J. Mohammad, K. Cantrell, C.U. Pittman, Pyrolysis of Wood and Bark in an Auger Reactor: Physical Properties and Chemical Analysis of the Produced Bio-oils, Energy Fuels. 22 (2008) 614–625. https://doi.org/10.1021/ef700335k.

[40] J.-L. Zheng, Pyrolysis oil from fast pyrolysis of maize stalk, Journal of Analytical and Applied Pyrolysis. 83 (2008) 205–212. https://doi.org/10.1016/j.jaap.2008.08.005.

[41] J. Zheng, W. Yi, N. Wang, Bio-oil production from cotton stalk, Energy Conversion and Management. 49 (2008) 1724–1730. https://doi.org/10.1016/j.enconman.2007.11.005.

[42] C.A. Mullen, A.A. Boateng, N.M. Goldberg, I.M. Lima, D.A. Laird, K.B. Hicks, Bio-oil and bio-char production from corn cobs and stover by fast pyrolysis, Biomass and Bioenergy. 34 (2010) 67–74. https://doi.org/10.1016/j.biombioe.2009.09.012.

[43] Q. Lu, J. Zhang, X. Zhu, Corrosion properties of bio-oil and its emulsions with diesel, Chin. Sci. Bull. 53 (2008) 3726–3734. https://doi.org/10.1007/s11434-008-0499-7.

[44] B. Scholze, Long-term stability, catalytic upgrading, and applicaton of pyrolysis oils : improving the properties of a potential substitute for fossil fuels, University of Hamburg, 2002.

[45] P. Basu, Chapter 14 - Analytical Techniques, in: P. Basu (Ed.), Biomass Gasification, Pyrolysis and Torrefaction (Third Edition), Academic Press, 2018: pp. 479–495. https://doi.org/10.1016/B978-0-12-812992-0.00023-6.

[46] S. Zhang, Y. Yan, T. Li, Z. Ren, Upgrading of liquid fuel from the pyrolysis of biomass, Bioresource Technology. 96 (2005) 545–550. https://doi.org/10.1016/j.biortech.2004.06.015.

[47] C.A. Mullen, A.A. Boateng, K.B. Hicks, N.M. Goldberg, R.A. Moreau, Analysis and Comparison of Bio-Oil Produced by Fast Pyrolysis from Three Barley Biomass/Byproduct Streams, Energy Fuels. 24 (2010) 699–706. https://doi.org/10.1021/ef900912s.

[48] A.A. Boateng, D.E. Daugaard, N.M. Goldberg, K.B. Hicks, Bench-Scale Fluidized-Bed Pyrolysis of Switchgrass for Bio-Oil Production †, Ind. Eng. Chem. Res. 46 (2007) 1891–1897. https://doi.org/10.1021/ie0614529.

[49] C. Brown, The outlook for future wood supply from forest plantations, FAO, Forestry Policy and Planning Division, Rome, 2000. http://www.fao.org/3/X8423E/X8423E00.htm#TopOfPage (accessed July 28, 2020).

[50] A. Portin, P. Lehtonen, Strategic review on the future of forest plantations, Forest Steward Council, Indufor Oy, Helsinki, Finland, 2012.

[51] L. Ugalde, O. Pérez, Mean annual volume increment of selected industrial forest plantation species, FAO, Forestry Department, Rome, Italy, 2001.

[52] T. Kaipainen, J. Liski, A. Pussinen, T. Karjalainen, Managing carbon sinks by changing rotation length in European forests, Environmental Science & Policy. 7 (2004) 205–219. https://doi.org/10.1016/j.envsci.2004.03.001.

[53] A.A. Myburg, D. Grattapaglia, G.A. Tuskan, U. Hellsten, R.D. Hayes, J. Grimwood, J. Jenkins, E. Lindquist, H. Tice, D. Bauer, D.M. Goodstein, I. Dubchak, A. Poliakov, E. Mizrachi, A.R.K. Kullan, S.G.

Hussey, D. Pinard, K. van der Merwe, P. Singh, I. van Jaarsveld, O.B. Silva-Junior, R.C. Togawa, M.R. Pappas, D.A. Faria, C.P. Sansaloni, C.D. Petroli, X. Yang, P. Ranjan, T.J. Tschaplinski, C.-Y. Ye, T. Li, L. Sterck, K. Vanneste, F. Murat, M. Soler, H.S. Clemente, N. Saidi, H. Cassan-Wang, C. Dunand, C.A. Hefer, E. Bornberg-Bauer, A.R. Kersting, K. Vining, V. Amarasinghe, M. Ranik, S. Naithani, J. Elser, A.E. Boyd, A. Liston, J.W. Spatafora, P. Dharmwardhana, R. Raja, C. Sullivan, E. Romanel, M. Alves-Ferreira, C. Külheim, W. Foley, V. Carocha, J. Paiva, D. Kudrna, S.H. Brommonschenkel, G. Pasquali, M. Byrne, P. Rigault, J. Tibbits, A. Spokevicius, R.C. Jones, D.A. Steane, R.E. Vaillancourt, B.M. Potts, F. Joubert, K. Barry, G.J. Pappas, S.H. Strauss, P. Jaiswal, J. Grima-Pettenati, J. Salse, Y. Van de Peer, D.S. Rokhsar, J. Schmutz, The genome of Eucalyptus grandis, Nature. 510 (2014) 356–362. https://doi.org/10.1038/nature13308.

[54] D.L. Klass, Chapter 8 - Thermal Conversion: Pyrolysis and Liquefaction, in: D.L. Klass (Ed.), Biomass for Renewable Energy, Fuels, and Chemicals, Academic Press, San Diego, 1998: pp. 225–269. https://doi.org/10.1016/B978-012410950-6/50010-6.

[55] J. Xu, Y. Liao, Y. Lin, X. Ma, Z. Yu, Study on catalytic pyrolysis of eucalyptus to produce aromatic hydrocarbons by Zn-Fe co-modified HZSM-5 catalysts, Journal of Analytical and Applied Pyrolysis. 139 (2019) 96–103. https://doi.org/10.1016/j.jaap.2019.01.014.

[56] S. Yanik, R. Bartek, P. O'Connor, D. Stamires, M. Brady, Biomass conversion process, US20100105970A1, 2010. https://patents.google.com/patent/US20100105970A1/en (accessed July 28, 2020).

[57] P.T. Hang, G.W. Brindley, Methylene Blue Absorption by Clay Minerals. Determination of Surface Areas and Cation Exchange Capacities (Clay-Organic Studies XVIII), Clays Clay Miner. 18 (1970) 203–212. https://doi.org/10.1346/CCMN.1970.0180404.

[58] F.J.W.J. Labuschagne, E.W. Giesekke, J.D.V. Schalkwyk, Production of hydrotalcite, WO2006123284A2, 2006. https://patents.google.com/patent/WO2006123284A2/en?q=production+hydrotalcite&inventor=labuschagne&oq=production+of+hydrotalcite+labuschagne (accessed August 9, 2020).

[59] P.-H. Chang, Y.-P. Chang, Y.-H. Lai, S.-Y. Chen, C.-T. Yu, Y.-P. Chyou, Synthesis, characterization and high temperature CO2 capture capacity of nanoscale Ca-based layered double hydroxides via reverse microemulsion, Journal of Alloys and Compounds. 586 (2014) S498–S505. https://doi.org/10.1016/j.jallcom.2013.05.213.

[60] M. Laipan, R. Zhu, Q. Chen, J. Zhu, Y. Xi, G.A. Ayoko, H. He, From spent Mg/Al layered double hydroxide to porous carbon materials, Journal of Hazardous Materials. 300 (2015) 572–580. https://doi.org/10.1016/j.jhazmat.2015.07.057.

[61] R.D. Merckel, W.W. Focke, M.M. Sibanda, P.M. Jr, N.A.S. Crowther, Co-Intercalation of Insecticides with Hexadecyltrimethylammonium Chloride in Mozambican Bentonite, Molecular Crystals and Liquid Crystals. 555 (2012) 76–84. https://doi.org/10.1080/15421406.2012.634682.

[62] K.H. Kim, T.-S. Kim, S.-M. Lee, D. Choi, H. Yeo, I.-G. Choi, J.W. Choi, Comparison of physicochemical features of biooils and biochars produced from various woody biomasses by fast pyrolysis, Renewable Energy. 50 (2013) 188–195. https://doi.org/10.1016/j.renene.2012.06.030.

[63] J. Jae, G.A. Tompsett, A.J. Foster, K.D. Hammond, S.M. Auerbach, R.F. Lobo, G.W. Huber, Investigation into the shape selectivity of zeolite catalysts for biomass conversion, Journal of Catalysis. 279 (2011) 257–268. https://doi.org/10.1016/j.jcat.2011.01.019.